frontiers in Microbiology

ORIGINAL RESEARCH
published: 14 December 2021
doi: 10.3389/fmicb.2021.795047

The HBV Core Protein and Core Particle Both Bind to the PPIase Par14 and Par17 to Enhance Their Stabilities and HBV Replication

*Umar Saeed[1,2], Zahra Zahid Piracha[1,2], Hyeonjoong Kwon[1,2], Jumi Kim[1,2], Fadia Kalsoom[1,2], Yong-Joon Chwae[1,2], Sun Park[1,2], Ho-Joon Shin[1,2], Hyun Woong Lee[3], Jin Hong Lim[4] and Kyongmin Kim[1,2]**

[1]Department of Microbiology, Ajou University School of Medicine, Suwon, South Korea, [2]Department of Biomedical Science, Graduate School of Ajou University, Suwon, South Korea, [3]Department of Internal Medicine, Gangnam Severance Hospital, Yonsei University College of Medicine, Seoul, South Korea, [4]Department of General Surgery, Gangnam Severance Hospital, Yonsei University College of Medicine, Seoul, South Korea

OPEN ACCESS

Edited by:
Douglas Paul Gladue, United States Department of Agriculture, United States

Reviewed by:
Xupeng Hong, The Pennsylvania State University, United States
Lin Deng, Kobe University, Japan

***Correspondence:**
Kyongmin Kim
kimkm@ajou.ac.kr

Specialty section:
This article was submitted to Virology, a section of the journal Frontiers in Microbiology

Received: *14 October 2021*
Accepted: *17 November 2021*
Published: *14 December 2021*

Citation:
Saeed U, Piracha ZZ, Kwon H, Kim J, Kalsoom F, Chwae Y-J, Park S, Shin H-J, Lee HW, Lim JH and Kim K (2021) The HBV Core Protein and Core Particle Both Bind to the PPIase Par14 and Par17 to Enhance Their Stabilities and HBV Replication. Front. Microbiol. 12:795047. doi: 10.3389/fmicb.2021.795047

We recently reported that the PPIase Par14 and Par17 encoded by *PIN4* upregulate HBV replication in an HBx-dependent manner by binding to conserved arginine–proline (RP) motifs of HBx. HBV core protein (HBc) has a conserved ^{133}RP^{134} motif; therefore, we investigated whether Par14/Par17 bind to HBc and/or core particles. Native agarose gel electrophoresis (NAGE) and immunoblotting and co-immunoprecipitation were used. Chromatin immunoprecipitation from HBV-infected HepG2-hNTCP-C9 cells was performed. NAGE and immunoblotting revealed that Par14/Par17 bound to core particles and co-immunoprecipitation revealed that Par14/Par17 interacted with core particle assembly-defective, and dimer-positive HBc-Y132A. Thus, core particles and HBc interact with Par14/Par17. Par14/Par17 interacted with the HBc ^{133}RP^{134} motif possibly *via* substrate-binding E46/D74 and E71/D99 motifs. Although Par14/Par17 dissociated from core particles upon heat treatment, they were detected in 0.2 N NaOH-treated opened-up core particles, demonstrating that Par14/Par17 bind outside and inside core particles. Furthermore, these interactions enhanced the stabilities of HBc and core particles. Like HBc-Y132A, HBc-R133D and HBc-R133E were core particle assembly-defective and dimer-positive, demonstrating that a negatively charged residue at position 133 cannot be tolerated for particle assembly. Although positively charged R133 is solely important for Par14/17 interactions, the ^{133}RP^{134} motif is important for efficient HBV replication. Chromatin immunoprecipitation from HBV-infected cells revealed that the S19 and E46/D74 residues of Par14 and S44 and E71/D99 residues of Par17 were involved in recruitment of ^{133}RP^{134} motif-containing HBc into cccDNA. Our results demonstrate that interactions of HBc, Par14/Par17, and cccDNA in the nucleus and core particle–Par14/Par17 interactions in the cytoplasm are important for HBV replication.

Keywords: Hepatitis B virus, HBV replication study, PPIase activity, parvulin 14, parvulin 17

INTRODUCTION

HBV is a prototype virus in the *Hepadnaviridae* family with a partially double-stranded, relaxed-circular (RC) DNA genome that shows exclusive tropism for hepatocytes (Seeger and Mason, 2015) HBV infection causes acute hepatitis, which can lead to chronic hepatitis B, liver fibrosis, cirrhosis, and hepatocellular carcinoma (Seeger and Mason, 2015). Currently available treatments cannot cure HBV infection (Cornberg and Manns, 2018; Revill et al., 2019). In total, 257 million people are living with chronic hepatitis B (World Health Organization Gobal Heptatitis report, 2017).

HBV infects hepatocytes by binding to heparan sulfate, followed by the sodium taurocholate cotransporting polypeptide (SLC10A1 or NTCP) receptor (Yan et al., 2012). Incoming core particle (capsid or nucleocapsid) moves to the nuclear pore complex and releases its genome into the nucleus. There, the polymerase-bound RC DNA genome is converted to covalently closed circular DNA (cccDNA) *via* several host proteins (Diab et al., 2018; Mohd-Ismail et al., 2019). The cccDNA minichromosome serves as a template for transcription of viral genes. The episomal cccDNA contains four overlapping open reading frames, which transcribe 3.5 kb pregenomic RNA (pgRNA) encoding HBc (core) and polymerase proteins, 2.4 and 2.1 kb S mRNAs producing large, middle, and small surface (HBs) proteins, and 0.7 kb X mRNA encoding HBx protein (Ganem, 2001; Hu and Seeger, 2015; Seeger and Mason, 2015).

The 21 KDa HBc protein consists of 183 and 185 amino acids in the ayw and adw subtypes, respectively, and has three domains, namely, the N-terminal domain (NTD) (Birnbaum and Nassal, 1990), linker domain (Watts et al., 2002), and C-terminal domain (CTD; Birnbaum and Nassal, 1990). The NTD (140 amino acids) is critical and sufficient for core particle assembly (Gallina et al., 1989; Birnbaum and Nassal, 1990). The linker domain (nine amino acids) performs critical roles during multiple stages of HBV replication (Liu et al., 2018). The CTD (34 [ayw] or 36 [adw] amino acids) is dispensable for capsid assembly, but plays important roles in pgRNA packaging and reverse transcription (Yu and Summers, 1991; Nassal, 1992; Köck et al., 2004; Jung et al., 2012). Through post-translational modifications of the CTD, HBc plays versatile roles in multiple stages of the HBV life cycle, including core particle assembly, reverse transcription, modulation of cccDNA transcription *via* epigenetic regulation (Jung et al., 2014; Zlotnick et al., 2015; Diab et al., 2018). HBc has reemerged as a promising anti-HBV target (Venkatakrishnan and Zlotnick, 2016; Xie et al., 2017; Diab et al., 2018).

Crystallography of C-terminally truncated HBc protein demonstrated that it contains five α-helices, among which helices 3 and 4 form an α-helical hairpin structure (Wynne et al., 1999). The α-helical hairpin further assembles into dimers and forms a four-helix bundle. Afterward, the trimers of dimers further assemble into hexamers to form HBV core particles (Birnbaum and Nassal, 1990). The HBV core particle is assembled *via* dimeric intermediates of HBc (Hatton et al., 1992; Bourne et al., 2009) and is thus composed of 90 or 120 HBc dimers depending on whether T = 3 or T = 4, respectively (Zlotnick et al., 1996).

The core particle incorporates pgRNA and polymerase containing reverse transcriptase and facilitates synthesis of DNA. The core particle with RC DNA is subsequently enveloped by HBs proteins as infectious virion (Hu and Seeger, 2015; Zlotnick et al., 2015; Venkatakrishnan and Zlotnick, 2016) or alternatively trafficked back to the nucleus and maintains the cccDNA pool (Ko et al., 2018).

Peptidyl-prolyl cis/trans isomerases (PPIases) regulate protein folding and functions by inducing cis/trans isomerization of target proteins (Göthel and Marahiel, 1999; Lu et al., 2007). There are four families of PPIases, namely, cyclophilins, FK506-binding proteins, parvulins, and protein Ser/Thr phosphatase 2A activator (Lu et al., 2007). Among parvulins, the *PIN1* gene encodes the PPIase NIMA-interacting 1 (Pin1) protein, while the *PIN4* gene encodes the Par14 and Par17 proteins (Lu et al., 1996; Rulten et al., 1999; Mueller et al., 2006). Par14/Par17 regulate cell cycle progression, chromatin remodeling, ribosomal RNA processing, and tubulin polymerization (Thiele et al., 2011; Saningong and Bayer, 2015; Matena et al., 2018).

We recently reported that Par14/Par17 are involved in the HBV life cycle. They are recruited to the HBV cccDNA and thereby augment HBV RNA transcription and DNA synthesis in an HBx-dependent manner (Saeed et al., 2019). Considering the importance of the RP motifs of HBx for Par14/Par17–HBx interactions in HBV replication (Saeed et al., 2019), we asked whether the RP motif of HBc is critical for its interaction with Par14/Par17 and HBV replication. Here, we found that Par14/Par17 are bona-fide binding partners of both HBc and the core particle. The Par14/Par17–HBc and/or –core particle interactions improved the stabilities of HBc and core particles. Similar to HBx–Par14/Par17–cccDNA interactions in the nucleus (Saeed et al., 2019), Par14/Par17 can directly bind to cccDNA, simultaneously associate with HBc, and promote HBV replication from cccDNA *via* transcriptional activation.

MATERIALS AND METHODS

Vector Construction

The human NTCP-C9 construct, pCDH-hNTCP-C9, was previously described (Piracha et al., 2018, 2020; Saeed et al., 2019) and generated by inserting hNTCP-C9 into pcDNA6.1 (a kind gift from Dr. Li W; Yan et al., 2012). The pCMV-3 × FLAG-tagged Par14 WT, -Par17 WT, -Par14-E46A/D74A, and -Par17-E71A/D99A constructs and short hairpin RNAs (shPIN4-#1, shPIN4-#5, and shControl) in pLK0.1 were described previously (Saeed et al., 2019). To construct Myc-tagged HBc WT, PCR-amplified HBc DNA (**Table 1**) was digested with *Msc*I and *Kpn*I and inserted into the

Abbreviations: HBV, hepatitis B virus; PPIase, peptidyl-prolyl cis/trans isomerases; Par14, parvulin 14; Par17, parvulin 17; NAGE, native agarose gel electrophoresis; cccDNA, covalently closed circular DNA; SDS-PAGE, sodium dodecyl sulfate polyacrylamide gel electrophoresis; ChIP, chromatin immunoprecipitation; NIRF, Np95/ICBP90-like RING finger protein; PRMT5, protein arginine methyltransferase 5; CREB, cAMP response element-binding protein.

TABLE 1 | Primers used in this study.

	Plasmid		Sequence (5′-3′)
HBc	Myc-HBc	F	CTTATGGCCACGGACATTGACCCT
		R	ATTGGTACCCTAACATTGAGATT
HBc mutants	HBc-Y132A	F	CTC CTC CAG CC*G C*TA GAC CAC CAA A
		R	TTT GGT GGT CTA *GC*G GCT GGA GGA G
	HBc-R133A	F	ACT CCT CCA GCC TAT *GC*A CCA CCA AAT GCC CCT
		R	AGG GGC ATT TGG TGG T*GC* ATAGGCTGGAGGAGT
	HBc-R133D	F	ACT CCT CCA GCC TAT *GAT* CCA CCA AAT GCC CCT
		R	AGG GGC ATT TGG TGG *ATC* ATA GGC TGG AGG AGT
	HBc-R133E	F	ACT CCT CCA GCC TAT *GAA* CCA CCA AAT GCC CCT
		R	AGG GGC ATT TGG TGG T*TC* ATA GGC TGG AGG AGT
	HBc-R133K	F	ACT CCT CCA GCC TAT *AA*A CCA CCA AAT GCC CCT
		R	AGG GGC ATT TGG TGG T*TT* ATA GGC TGG AGG AGT
	HBc-R133L	F	CCT CCA GCC TAT *CT*A CCA CCA AAT GCC
		R	GGC ATT TGG TGG T*AG* ATA GGC TGG AGG
	HBc-R133H	F	CCT CCA GCC TAT *CAT* CCA CCA AAT GCC
		R	GGC ATT TGG TGG *ATG* ATA GGC TGG AGG
	HBc-P134A	F	CCA GCC TAT AGA *G*CA CCA AAT GCC CCT
		R	AGG GGC ATT TGG TG*C* TCT ATA GGC TGG
	HBc-AAP	F	CCT CCA GCC TAT *GC*A *G*CA CCA AAT GCC
		R	GGC ATT TGG TG*C* T*GC* ATA GGC TGG AGG
	HBc-RAA	F	CCA GCC TAT AGA *G*CA *G*CA AAT GCC CCT ATC
		R	GAT AGG GGC ATT TG*C* TG*C* TCT ATA GGC TGG
	HBc-AAA	F	CCT CCA GCC TAT *GC*A *G*CA *G*CA AAT GCC CCT
		R	AGG GGC ATT TG*C* TG*C* T*GC* ATA GGC TGG AGG
	pPB X def-1	F	CAT CGT TTC C*T*T GGC TGC TAG GTT GTA CTG
		R	CTA GCA GCC A*A*G GAA ACG ATG TAT AT
	pPB X def-2	F	CTC TGC ACG TTG C*T*T GGA GAC CAC CGT G
HBc- and HBx- deficient HBV constructs		R	CAC GGT GGT CTC CA*A* GCA ACG TGC AGA G
	pPB X def-3	F	CTT GGA CTC CCA GCA *T*TG TCA ACG ACC GAC
		R	GTC GGT CGT TGA CA*A* TGC TGG GAG TCC AAG
	HBc- and HBx- deficient	F	GAC CCT TAT AAA *T*AA TTT GGA GCT ACT GTG
HBV-HBc RP mutant		R	GTA GCT CCA AAT T*A*T TTA TAA GGG TCA ATG TC
	HBV-HBc-AAP	F	CATCAAGTGTATCATATGCCAAGTACGC
		R	CAAGAATATGGTGACCCGCAAAATGATG
	cccDNA	F	CTCCCCGTCTGTGCCTTCT
		R	GCCCCAAAGCCACCCAAG
	Actin	F	CATGTACGTTGCTATCCAGGC
		R	CTCCTTAATGTCACGCACGAT

1. F, forward; R, reverse.

linearized pCMV-Myc vector (Addgene #631604), yielding Myc-HBc WT. Using the mutagenic primers listed in **Table 1**, the respective *Msc*I/*Kpn*I-digested PCR products were inserted into the pCMV-Myc vector, yielding pCMV-Myc-HBc-Y132A (TAT → GCT), -R133A (AGA → GCA), -R133D (AGA → GAT), −R133E (AGA → GAA), -R133K (AGA → AAA), −R133L (AGA → CTA), -R133H (AGA → CAT), -P134A (CCA → GCA), -AAP (AGACCA→ GCAGCA), −RAA (CCACCA→GCAGCA), and -AAA (AGACCACCA→GCAGCAGCA). The HBV WT subtype adwR9 in pcDNA3.1 (Invitrogen), designated pPB, in which pgRNA transcription is under the control of the CMV IE promoter, was previously described (Kim et al., 2004). The HBc-deficient HBV construct with a stop codon (TAA) at amino acid 8 of HBc (Jung et al., 2012) and the HBx-deficient HBV construct with three ATG codons changed to TTG were generated using the pPB construct and described previously (**Table 1**; Yoon et al., 2011). HBc-deficient mutant HBV was generated using the HBx-deficient mutant HBV construct (**Table 1**), yielding the double-deficient HBc-HBx-deficient HBV construct. To generate the HBV construct with HBc-AAP, PCR-amplified HBc-AAP DNA (**Table 1**) was digested with *Nde*I/*BsTe*II and ligated into the *Nde*I/*BsTe*II-digested pPB construct, yielding the HBV-HBc-AAP mutant. All constructs generated by site-directed mutagenic PCR were sequenced to confirm the presence of specific mutations and the absence of extraneous mutations.

Cell Culture and DNA Transfection

Huh7, HepG2, HepG2-hNTCP-C9, HepAD38, and HEK293T cells were maintained in Dulbecco's modified Eagle's medium supplemented with 10% fetal bovine serum (Gibco BRL) and 1% penicillin–streptomycin in a humidified atmosphere (at 37°C in 5% CO_2), and passaged as described previously (Saeed et al., 2019). For transfection of Huh7 or HepG2 cells, 4 µg of the plasmid construct was mixed with 12 µg/µl polyethylenimine (PEI, Polysciences) and 200 µl of Opti-MEM (Gibco) and added to 2×10^6 cells in a 6 cm plate at 24 h after seeding. For co-transfection, 4 µg of 3×FLAG-Par14/Par17 WT or mutants plus 4 µg of Myc-HBc WT or mutants were mixed with 24 µg/µl PEI and 200 µl of Opti-MEM and the mixtures were added to cells as described above. For quadruple transfection, 3 µg of the HBc-HBx-deficient construct plus 3 µg of 3×FLAG-Par14/Par17 WT or mutants plus 3 µg of Myc-HBc WT or Myc-HBc-AAP plus 3 µg of Myc-HBx WT or Myc-HBx-AAAA were mixed with 24 µg/µl PEI and 200 µl of Opti-MEM and the mixtures were added to cells as described above. To ensure the same amount of DNA was transfected in each experimental setup, the amount of DNA was adjusted using the pCMV empty vector.

Establishment of Stable Cell Lines

HepG2-hNTCP-C9 stable cells were generated as described previously (Nkongolo et al., 2014; Piracha et al., 2018, 2020; Saeed et al., 2019). The lentiviral vector system was used to generate Huh7, HepG2, and HepG2-hNTCP-C9-derived *PIN4* KD cells as described previously (Saeed et al., 2019). HepG2-hNTCP-C9 cells stably overexpressing Par14 or Par17 were described previously (Saeed et al., 2019).

HBc Amino Acid Sequence Alignment

The following HBc amino acid sequences were randomly selected from the National Center for Biotechnology Information gene database: 10 (A–J) human HBV genotypes; other mammalian hepadnaviruses including chimpanzee HBV, ground squirrel hepatitis virus, orangutan HBV, woodchuck hepatitis virus, and woolly monkey HBV; and avian hepadnaviruses, such as duck HBV, heron HBV, ross goose HBV, snow goose HBV, and stork HBV. The HBc amino acid sequences were fed into the CLC Main Workbench 8 software (CLC Main Workbench 21.0 software, 2021) to generate representative consensus sequences and conservation graphs.

Core Particle Immunoblotting, SDS-Page, and Western Blotting

Cells were lysed using 0.2% NP-40 (IGEPAL, Sigma-Aldrich)-TNE buffer (10 mM Tris–HCl [pH 8.0], 50 mM NaCl, and 1 mM EDTA) as described previously (Kim et al., 2004). Equal quantities of cell lysates measured by the Bradford assay were subjected to 13.5% SDS-PAGE. For reducing SDS-PAGE, sample buffer containing 125 mM Tris–HCl, pH 6.8, 20% glycerol, 4% SDS, 0.1% bromophenol blue, and 5% β-mercaptoethanol was used (Cold Spring Harbor Laboratory, 2015a). For non-reducing PAGE, sample buffer was as described above except that 5% β-mercaptoethanol was omitted (Cold Spring Harbor Laboratory, 2015b). To analyze core particles by immunoblotting, 4% of total lysates were electrophoresed in 1% native agarose gels. To analyze Par14/Par17 binding to core particles, lysates of Huh7 cells co-transfected with 3×FLAG-Par14/Par17 plus Myc-HBc were prepared at 72 h post-transfection. To detach Par14/Par17 binding outside the core particle, lysates were heated at 65°C for 2 h. Core particles were precipitated with 6% PEG (Kim et al., 2004), washed with 0.2% NP-40-TNE buffer to thoroughly remove Par14/Par17 detached from core particles. Thereafter, core particles were pelleted with 6% PEG, re-suspended in TNE buffer, and subjected to SDS-PAGE plus immunoblotting and NAGE plus immunoblotting. To detect Par14/Par17 proteins inside the core particle, core particles transferred to the PVDF membrane were treated with 0.2% NaOH for 40 s to open-up core particles and UV-crosslinked. By doing so, Par14/Par17 proteins inside the core particle could be detected by immunoblotting with mouse monoclonal anti-FLAG M2 (1:1,000, Sigma #F1804), rabbit monoclonal anti-PIN4 (1:1,000, Abcam #ab155283), and rabbit polyclonal anti-HBc (1:1,000, generated in-house) antibodies (Jung et al., 2012). Resolved proteins or core particles transferred to PVDF membranes were incubated overnight with primary antibodies (anti-FLAG, anti-PIN4, anti-HBc, and rabbit polyclonal anti-Myc [1:1,000, Santa Cruz Biotech #sc-789]; mouse monoclonal anti-GAPDH [1:5,000, Santa Cruz #sc-32233]; or rabbit polyclonal anti-H3 [1:5,000, Abcam #ab1791]), followed by an anti-rabbit or anti-mouse secondary antibody coupled to horseradish peroxidase (1:5,000, Thermo Fisher Scientific). The immunoblots were visualized by enhanced chemiluminescence (ECL Western blotting detection reagent, Amersham). Relative intensities were calculated using ImageJ v.1.46r.

Co-immunoprecipitation

To examine Par14/Par17 and HBc interactions, lysates of 2×10^6 Huh7 cells were prepared at 72 h after transfection. Cell lysates were immunoprecipitated with a rabbit polyclonal anti-Myc antibody (1:1,000, Santa Cruz Biotechnology #sc-789) and immunoblotted with a mouse monoclonal anti-FLAG antibody (Sigma #F1804) or vice versa. Normal rabbit IgG (Merck Millipore #12-370) or normal mouse IgG (Merck Millipore #12-371) was used as a negative control for immunoprecipitation. The lysates were subjected to 16.5% SDS-PAGE and transferred to PVDF membranes for immunoblotting with a primary antibody (anti-Myc, anti-FLAG, or anti-GAPDH), followed by an anti-rabbit or anti-mouse secondary antibody coupled to horseradish peroxidase. The immunoblots were visualized by enhanced chemiluminescence.

HBc Stability Analysis

PIN4-KD Huh7 cells (2×10^5) grown on 6-well plates were transfected with 0.5 µg of respective constructs using 2 µg/ml PEI in 100 µl of Opti-MEM. At 24 h post-transfection, the medium was replaced with fresh medium containing 100 µg/ml cycloheximide (Sigma #C1988-1G) and harvested 0, 6, 12, or 24 h later.

Northern and Southern Blotting

To analyze HBV RNA synthesis by Northern blotting, total RNA was extracted from HepG2-hNTCP-C9 cells using TRIzol reagent (Ambion, Invitrogen #15596026). Twenty micrograms of total RNA was denatured at 65°C for 10 min, electrophoresed on a 1.2% agarose gel (Ultrapure Agarose, Invitrogen #16500500) containing 1× MOPS buffer [10 mM EDTA, 200 mM MOPS, and 50 mM sodium acetate (pH 7.0)] and formaldehyde (Sigma-Aldrich #F8775), and transferred to a nylon membrane (Roche, Sigma-Aldrich #11417240001) as described previously (Kim et al., 2004; Saeed et al., 2019; Piracha et al., 2020). To analyze HBV DNA synthesis by Southern blotting, HBV DNA extracted from isolated core particles was separated by electrophoresis on a 1% native agarose gel and transferred to a nylon membrane (Whatman #10416296). HBV total RNAs or HBV DNAs were hybridized to a ^{32}P-labeled random-primed probe specific for full-length HBV for 4 h at 68°C and then subjected to autoradiography as described previously (Kim et al., 2004). For Northern and Southern blotting of infected cells, total RNA and lysates were prepared at 5 and 9 days post-infection (p.i.), respectively.

HBV Preparation and Infection

To infect hNTCP-C9-expressing HepG2 cells with HBV, HBV virions were prepared from HepAD38 cells, as described previously (Watashi et al., 2013; Nkongolo et al., 2014; Saeed et al., 2019; Piracha et al., 2020). For HBV infection, 2×10^5 HepG2-hNTCP-C9 and HepG2-hNTCP-C9-shControl, -shPIN4-#1, and -shPIN4-#5 cells on collagen-coated 6-well plates (Corning #354249) were infected with 1.7×10^3 GEq of HBV per cell in medium containing 4% PEG (Affymetrix #25322-68-3), as described previously (Ni et al., 2014; Saeed et al., 2019). To determine the effects of Par14/Par17 mutants on recruitment of HBc onto cccDNA, 2×10^5 HepG2, HepG2-hNTCP-C9, and HepG2-hNTCP-C9-shControl, -shPIN4-#1, and -shPIN4-#5 cells in collagen-coated 6-well plates were transfected with 0.5 μg of the respective Par14/Par17 WT or mutant constructs with 2 μg/ml PEI in 100 μl of Opti-MEM. At 24 h post-transfection, the medium was refreshed, and cells were infected with 1.7×10^3 GEq of HBV per cell. HBV WT or HBV-HBc-AAP mutant virions were prepared from HepG2 cells. Briefly, 5×10^6 HepG2 cells in collagen-coated 15 cm plates were transfected with 16 μg of the HBV WT or HBV-HBc-AAP construct using 64 μg/ml PEI in 400 μl of Opti-MEM. The cells were grown in Dulbecco's modified Eagle's medium supplemented with 10% fetal bovine serum, 1% penicillin–streptomycin, 5 μg/ml insulin, and 50 μM hydrocortisone hemisuccinate. The culture supernatants were collected every third day for 2 weeks, samples were pelleted using PEG, and HBV DNA was quantitated by Southern blotting as described previously (Saeed et al., 2019; Piracha et al., 2020). To recover the same amounts of virions for HBV-HBc-AAP compared with HBV WT, a 7-times larger volume of supernatant needed to be harvested for HBV-HBc-AAP. For infection, 2×10^5 HepG2-hNTCP-C9 cells, HepG2-hNTCP-C9 cells stably overexpressing Par14 or Par17, and HepG2-hNTCP-C9-shControl, -shPIN4-#1, and -shPIN4-#5 cells were plated as described above and infected with 1.7×10^3 GEq of HBV WT or HBV-HBc-AAP mutant virions per cell (Ni et al., 2014; Saeed et al., 2019; Piracha et al., 2020) Lysates were prepared at 9 days p.i. for SDS-PAGE and immunoblotting, core particle immunoblotting, cccDNA extraction, and ChIP analysis.

cccDNA Extraction

HBV cccDNA was extracted using the Hirt protein-free DNA extraction procedure, as described previously (Cai et al., 2013) with minor modifications (Saeed et al., 2019). In brief, 2×10^5 HepG2-hNTCP-C9, *PIN4*-KD HepG2-hNTCP-C9, or Par14- or Par17-overexpressing stable HepG2-hNTCP-C9 cells were infected with HBV as described in the "HBV preparation and infection" sub-section. At 9 days p.i, when cells had reached 100% confluency, lysates were prepared to extract cccDNA and Southern blotting was performed as described in the "Northern and Southern blotting" sub-section.

cccDNA Chip and PCR

HBV cccDNA ChIP analysis was performed (Belloni et al., 2009) with minor modifications as described previously (Saeed et al., 2019). Briefly, HBV-infected cells generated as described in the "HBV preparation and infection" sub-section were maintained for eight more days and lysed, and chromatin solutions were prepared as described previously (Belloni et al., 2009; Saeed et al., 2019). Crosslinked sonicated chromatin was subjected to immunoprecipitation with 3 μg of rabbit monoclonal anti-PIN4 (Abcam #ab155283), mouse monoclonal anti-FLAG M2 (Sigma #F1804), rabbit polyclonal anti-HBc (Jung et al., 2012), mouse monoclonal anti-RNA polymerase II (Abcam #ab817), rabbit polyclonal anti-AcH3 (Merck Millipore #06–599), and rabbit polyclonal anti-H3 (Abcam #ab1791) antibodies or normal mouse or rabbit IgG (negative controls) for 16 h at 4°C, incubated with protein A/G-plus agarose beads (Santa Cruz Biotechnology #sc-2003) overnight at 4°C, and centrifuged at 1,000 *g* for 5 min at 4°C to recover immunoprecipitated protein–DNA complexes. DNA was purified from the immunoprecipitated protein–DNA complexes as described previously (Belloni et al., 2009; Saeed et al., 2019). The DNA amount was adjusted to 50 ng after measurement of the OD_{260}. Actin levels (**Table 1**) were used to ensure equal loading of lysates. Immunoprecipitated chromatin was analyzed by semi-quantitative PCR (Applied Biosystems; GeneAmp PCR system 2700) or real-time quantitative PCR (Applied Biosystems by Thermo Fisher Scientific, QuantStudio 3 Real-Time PCR #A28131) using cccDNA-specific primers (Saeed et al., 2019; **Table 1**) according to the manufacturer's instruction (Merck Millipore, EZ ChIP 17-371).

RNase Protection Assay

To examine encapsidated pgRNA, core particles were isolated from HepG2 cells transfected with HBc WT or HBc RP motif mutants plus HBc-deficient HBV, as described previously (Kim et al., 2004). Total RNA was extracted as described

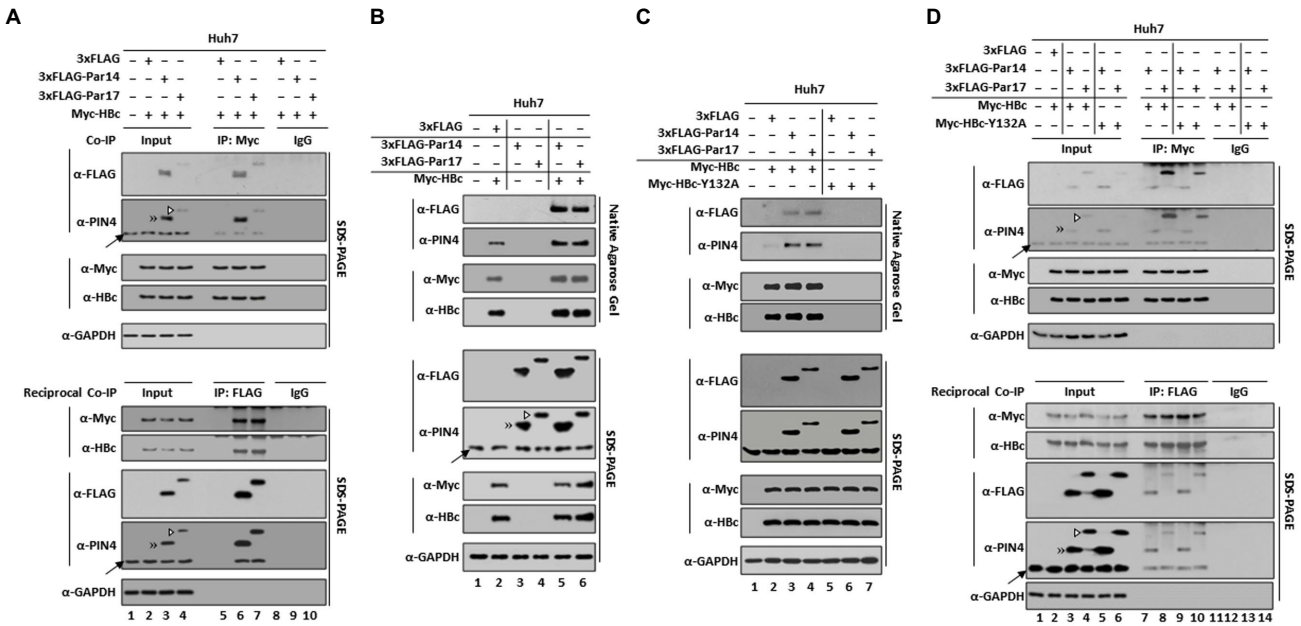

FIGURE 1 | Par14 and Par17 are novel binding partners of HBc and the core particle. **(A)** Co-immunoprecipitation reveals that Par14 and Par17 directly interact with the core particle and/or HBc of HBV. Huh7 cells in 6 cm plates were mock-transfected (lane 1) or co-transfected with 4 μg of Myc-HBc WT plus 3 × FLAG (lanes 2, 5, and 8), 3 × FLAG-Par14 WT (lanes 3, 6, and 9), or 3 × FLAG-Par17 WT (lanes 4, 7, and 10). At 72 h post-transfection, whole-cell lysates were prepared (lanes 1–4) and immunoprecipitated with an anti-Myc or anti-FLAG antibody (lanes 5–7). As a negative control, lysates were immunoprecipitated with normal rabbit IgG (Merck Millipore #12–370) or normal mouse IgG (Merck Millipore #12–371; lanes 8–10). SDS-PAGE and immunoblotting were performed. Resolved proteins were transferred to PVDF membranes and incubated overnight with mouse monoclonal anti-FLAG M2 (Sigma #F1804), rabbit monoclonal anti-PIN4 (1:1,000, Abcam #ab155283), rabbit polyclonal anti-Myc (Santa Cruz Biotech #sc-789), rabbit polyclonal anti-HBc (1:1,000, 17), and mouse monoclonal anti-GAPDH (1:5,000, Santa Cruz #sc-32,233) primary antibodies. GAPDH was used as a loading control. The blots were incubated with secondary antibodies (anti-mouse or anti-rabbit) coupled to horseradish peroxidase (1,5,000 dilution, Thermo Fisher Scientific). **(B)** NAGE and core particle immunoblotting reveal that the core particle of HBV interacts with Par14/Par17. Huh7 cells in 6 cm plates were mock-transfected (lane 1) or transfected with 3 × FLAG-Par14 WT (lane 3) or 3 × FLAG-Par17 WT (lane 4) or co-transfected with Myc-HBc WT plus 3 × FLAG (lane 2), 3 × FLAG-Par14 WT (lane 5), or 3 × FLAG-Par17 WT (lane 6). At 72 h post-transfection, cell lysates were prepared and subjected to 1% NAGE, transferred to a PVDF membrane, and immunoblotted with anti-FLAG, anti-PIN4, anti-Myc, and anti-HBc antibodies. **(C,D)** Both the HBV core particle and HBc interact with Par14/Par17. **(C)** NAGE and core particle immunoblotting demonstrate that HBc-Y132A is core particle assembly-defective, unlike HBc WT. Huh7 cells were mock-transfected (lane 1) or co-transfected with Myc-HBc WT or core particle assembly-defective Myc-HBc-Y132A plus 3 × FLAG (lanes 2 and 5), 3 × FLAG-Par14 WT (lanes 3 and 6), or 3 × FLAG-Par17 WT (lanes 4 and 7). **(D)** Co-immunoprecipitation reveals that Par14/Par17 directly interact with core particle assembly-defective HBc-Y132A. Lysates of transfected Huh7 cells were immunoprecipitated and subjected to SDS-PAGE as described above. The immunoblots were visualized by enhanced chemiluminescence (ECL Western blotting detection reagent, Amersham). Endogenous Par14 is marked with an arrow. Overexpressed Par14 and Par17 are marked with a double arrowhead and open arrowhead, respectively. A representative result from three independent experiments is shown.

above. The riboprobe was prepared as described previously (Kim et al., 2004; Piracha et al., 2020). Briefly, 446 nt of the digoxigenin (DIG)-UTP antisense probe was generated from the HBV sequence (nt 1,805–2,187) of the pGEM3Zf (+) plasmid (Kim et al., 2004) *in vitro* using SP6 RNA polymerase (Promega #P108B) with a kit (Roche #1363514). The RNase protection assay (RPA) procedure was conducted as described previously (Kim et al., 2004), except that labeling was performed with DIG (Piracha et al., 2020), according to the Roche protocol (Roche # 1363514, Roche #11585762001). Encapsidated and total RNAs (369 nt) following RNase digestion were electrophoresed on a 5% polyacrylamide-8 M urea gel and transferred to a nylon membrane (Roche, Sigma-Aldrich #11417240001). The membrane was incubated with an anti-DIG-AP antibody (1:1,000, Roche #11093274910) and visualized by the CSPD (Roche #11755633001) chemiluminescence reaction.

RESULTS

Par14 and Par17 Bind to Both HBc and the Core Particle of HBV

Par14 and Par17 bind to the RP motifs of HBx (Saeed et al., 2019); therefore, we reasoned that the single RP motif of HBc may serve as a binding site for Par14/Par17. To investigate whether HBc and/or the core particle can bind to Par14/Par17, co-immunoprecipitation and immunoblotting (**Figure 1A**) and NAGE and immunoblotting (**Figure 1B**) were performed. The anti-Myc and anti-FLAG antibodies immunoprecipitated Par14/Par17 and HBc, respectively (**Figure 1A**, lanes 6 and 7), demonstrating that HBc and/or the core particle can bind to Par14/Par17. NAGE and immunoblotting demonstrated that both Par14 and Par17 can physically interact with the core particle of HBV (**Figure 1B**, top and second panels, lanes 2, 5, and 6). Inhibition of

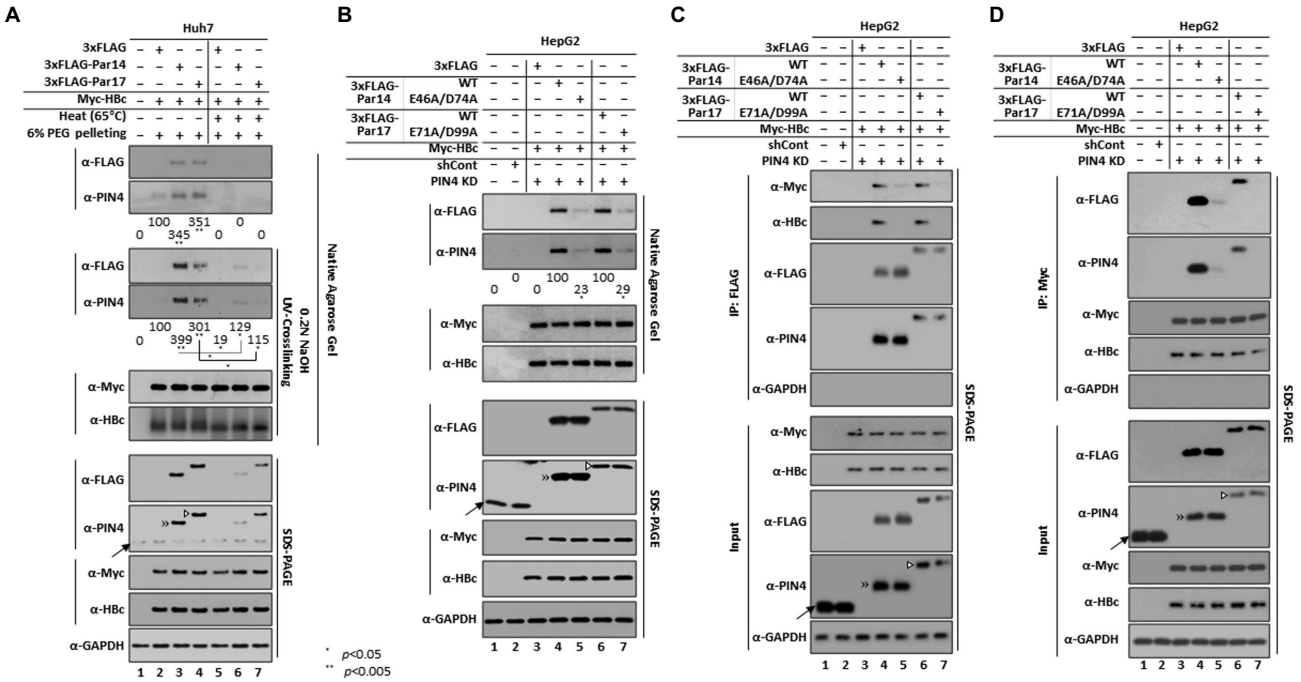

FIGURE 2 | Par14/Par17 bind both outside and inside the core particle, and the substrate-binding residues of Par14 (E46/D74) and Par17 (E71/D99) are critical for Par14/Par17–HBc and/or –core particle interactions. **(A)** Par14/Par17 bind both outside and inside HBV core particles. Huh7 cells were mock-transfected (lane 1) or co-transfected with Myc-HBc WT plus 3 × FLAG (lanes 2 and 5), 3 × FLAG-Par14 WT (lanes 3 and 6), or 3 × FLAG-Par17 WT (lanes 4 and 7). At 72 h post-transfection, lysates were left untreated (lanes 1–4) or heated at 65°C for 2 h (lanes 5–7). These core particles were precipitated with 6% PEG, washed, and re-precipitated with 6% PEG. The pellet was suspended in TNE buffer and subjected to NAGE plus immunoblotting and SDS-PAGE plus immunoblotting as described in **Figure 1**. The PVDF membrane containing core particles was treated with 0.2 N NaOH for 40 s, crosslinked with UV, and immunoblotted with anti-FLAG, anti-PIN4, anti-Myc, and anti-HBc antibodies. **(B–D)** E46/D74 of Par14 and E71/D99 of Par17 are important for interactions with the core particle. Non-transduced and mock-transfected (lane 1) and control shRNA-transduced (lane 2) HepG2 cells were used as controls. shPIN4-#1–transduced *PIN4*-KD HepG2 cells in 6 cm plates were co-transfected with Myc-HBc WT plus 3 × FLAG (lane 3), 3 × FLAG-Par14 WT (lane 4), 3 × FLAG-Par14-E46A/D74A (lane 5), 3 × FLAG-Par17 WT (lane 6), or 3 × FLAG-Par17-E71A/D99A (lane 7). **(C,D)** Lysates were immunoprecipitated with an anti-FLAG antibody and immunoblotted with an anti-Myc antibody **(C)** or vice versa **(D)**. At 72 h post-transfection, lysates were prepared. Lysates were subjected to NAGE and core particle immunoblotting as described **Figure 1B**. Input lysates and immunoprecipitants were also subjected to SDS-PAGE and immunoblotting as described in **Figures 1B–D**. Par14/Par17 bound to HBV core particles were measured using ImageJ v.1.46r. Representative results from three independent experiments are shown. Statistical significance was evaluated using Student's *t*-test. $^{*}p < 0.05$; $^{**}p < 0.005$ relative to the corresponding control (A and B).

parvulin with the competitive reversible inhibitor PiB (Uchida et al., 2003) or the competitive irreversible inhibitor juglone (Hennig et al., 1998; Chao et al., 2001) weakened the core particle–Par14/Par17 interactions (**Supplementary Figure S1**), suggesting they are dynamic on–off interactions. Consistently, heat treatment at 65°C weakened the core particle–Par14/Par17 interactions (**Supplementary Figure S2**).

This co-immunoprecipitation cannot discriminate Par14/Par17 binding to HBc, the core particle, or both; therefore, we examined the interactions of Par14/Par17 and HBc using a core particle assembly-defective dimer-positive HBc-Y132A mutant (Bourne et al., 2009). Consistent with a previous report, Myc-HBc-Y132A could not assemble into the core particle (**Figure 1C**, third and fourth panels, lanes 2–4 vs. 5–7; Bourne et al., 2009), although its expression was comparable with that of Myc-HBc WT (**Figure 1C**, seventh and eighth panels, lanes 2–4 vs. 5–7). Par14/Par17 were co-immunoprecipitated with HBc-Y132A (**Figure 1D**, lanes 9 and 10), demonstrating that HBc can bind to Par14/Par17. We conclude that both HBc and the core particle are binding partners of Par14/Par17.

Par14/Par17 Bind Both Outside and Inside Core Particles

Although Par14/Par17 can bind to the core particle based on the finding that they dissociated from it upon heat treatment at 65°C (**Supplementary Figure S2**), we could not exclude the possibility that Par14/Par17 may be incorporated into the core particle. To investigate that, cytoplasmic lysates were mock-treated or heated at 65°C for 2 h. As expected, heat treatment dissociated Par14/Par17 from outside the core particle (**Figure 2A**, top and second panels, lanes 2–4 vs. 5–7). Then, this membrane was treated with 0.2 N NaOH for 40 s to open-up core particles (Kim et al., 2004, 2008; Jung et al., 2014), ultraviolet (UV)-crosslinked, and immunoblotted. Although Par14/Par17 were dissociated from core particles by heat treatment, they were still detected in opened-up core particles (**Figure 2A**, third and fourth panels, lanes 5–7)

without any changes on to the core particle level (**Figure 2A**, fifth and sixth panels, lanes 2–7), indicating that Par14/Par17 are associated inside the core particle. Par14/Par17 were still detected by SDS-PAGE and immunoblotting after heat treatment, further supporting the above conclusion (**Figure 2A**, seventh and eighth panels, lanes 5–7). These results demonstrate that Par14/Par17 can bind to and be incorporated into the core particle.

The Substrate-Binding E46/71 and D74/99 Residues of Par14/Par17 Interact With HBc and/or the Core Particle

The negatively charged substrate-binding residues E46/71 and D74/99 of Par14/Par17 interact with the RP motifs of HBx (Saeed et al., 2019). Therefore, these residues of Par14/Par17 may also bind to the RP motif of HBc and/or the core particle. To exclude the effects of endogenous Par14/Par17, *PIN4* was knockdown (KD). NAGE and immunoblotting demonstrated that the substrate-binding-deficient Par14/Par17 mutants weakly interacted with the core particle (**Figure 2B**, top and second panels, lanes 4 vs. 5 and 6 vs. 7). The same lysates from **Figure 2B** were immunoprecipitated (**Figures 2C,D**). In accordance with **Figure 2B** (top and second panels), the E46A/D74A mutant of Par14 and E71A/D99A mutant of Par17 were not efficiently immunoprecipitated with HBc and/or the core particle (**Figures 2C,D**, top and second panels, lanes 4 vs. 5 and 6 vs. 7), indicating that the E46/71 and D74/99 of Par14/Par17 are important for the interactions with HBc and the core particle.

The HBc RP Motif Is Conserved Among Human, Mammalian, and Avian Hepadnaviruses

Par14/Par17 interacted with HBc and the core particle (**Figures 1, 2**); therefore, we reasoned that the positively charged amino acid preceding proline in HBc may be the interaction site of Par14/Par17 similar to HBx (Saeed et al., 2019). Sequence analysis of HBc revealed a single ^{133}RP^{134} motif in its NTD (**Figure 3A**). Amino acid sequence alignments of human HBc proteins demonstrated that among 16 XaaPro motifs, the ^{133}RP^{134} motif is completely conserved among 30 isolates from 10 genotypes (**Figure 3A**), indicating that the conserved RP motif is important for the HBV life cycle and/or viral pathogenesis. Furthermore, HBc proteins of mammalian and avian hepadnaviruses have a completely conserved RP motif (**Figures 3B,C**). The avian hepadnavirus

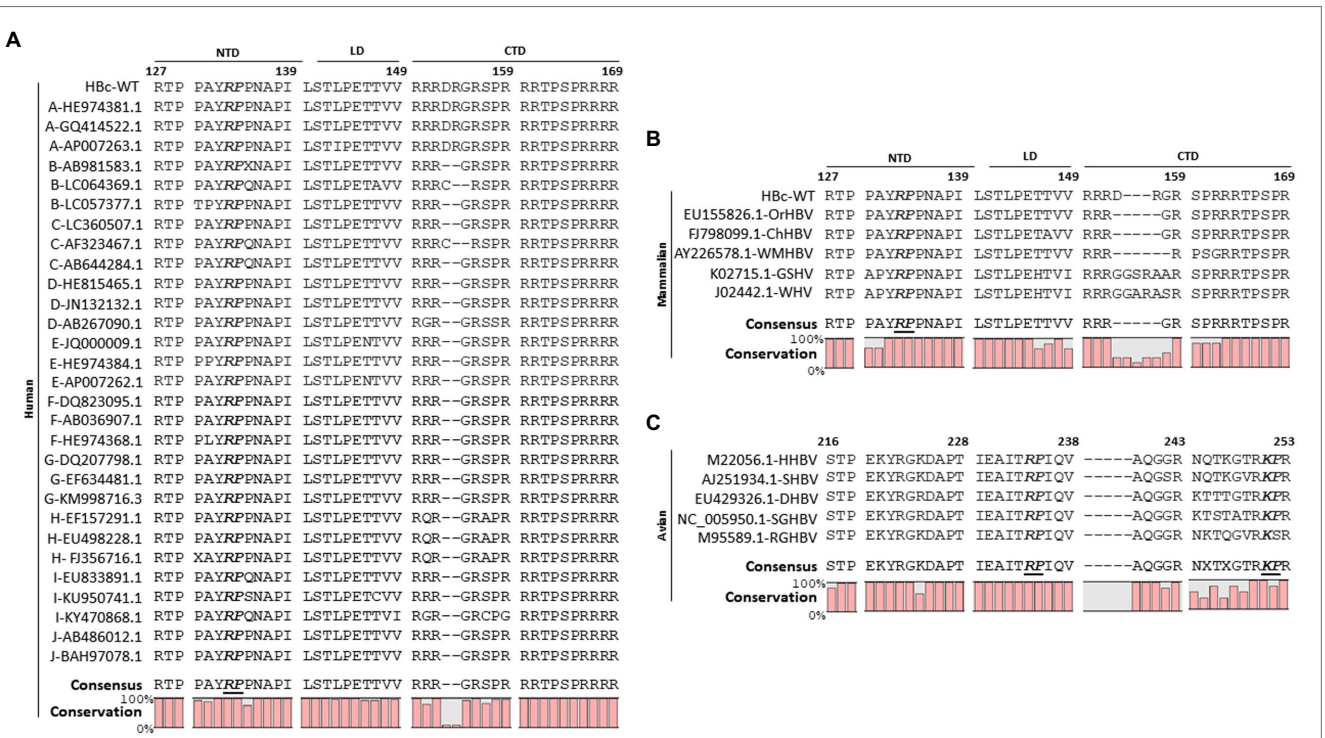

FIGURE 3 | The HBc ^{133}RP^{134} motif is conserved among human, mammalian, and avian hepadnaviruses. **(A)** The HBc ^{133}RP^{134} motif is completely conserved among isolates from 10 HBV genotypes including human HBV [adwR9 subtype (HBc WT)]. The partial NTD, linker, and partial CTD HBc amino acid sequences were aligned using CLC Main Workbench 8 software. The HBV genotype of each isolate is indicated in the left column, followed by accession numbers. **(B)** The mammalian HBc RP motif is completely conserved. The HBc amino acid sequences of orangutan HBV (OrHBV), chimpanzee HBV (ChHBV), woolly monkey HBV (WMHBV), ground squirrel hepatitis virus (GSHV), and woodchuck hepatitis virus (WHV) were aligned. **(C)** The avian HBc RP motif is completely conserved and an additional KP motif is also conserved. HBc amino acid sequences of heron HBV (HHBV), stork HBV (SHBV), duck HBV (DHBV), snow goose HBV (SGHBV), and ross goose HBV (RGHBV) were aligned. Accession numbers of mammalian and avian hepadnaviruses are presented. Conserved RP or KP motifs are shown in bold and italicized font. Consensus sequences and conservation percentages are shown at the bottom.

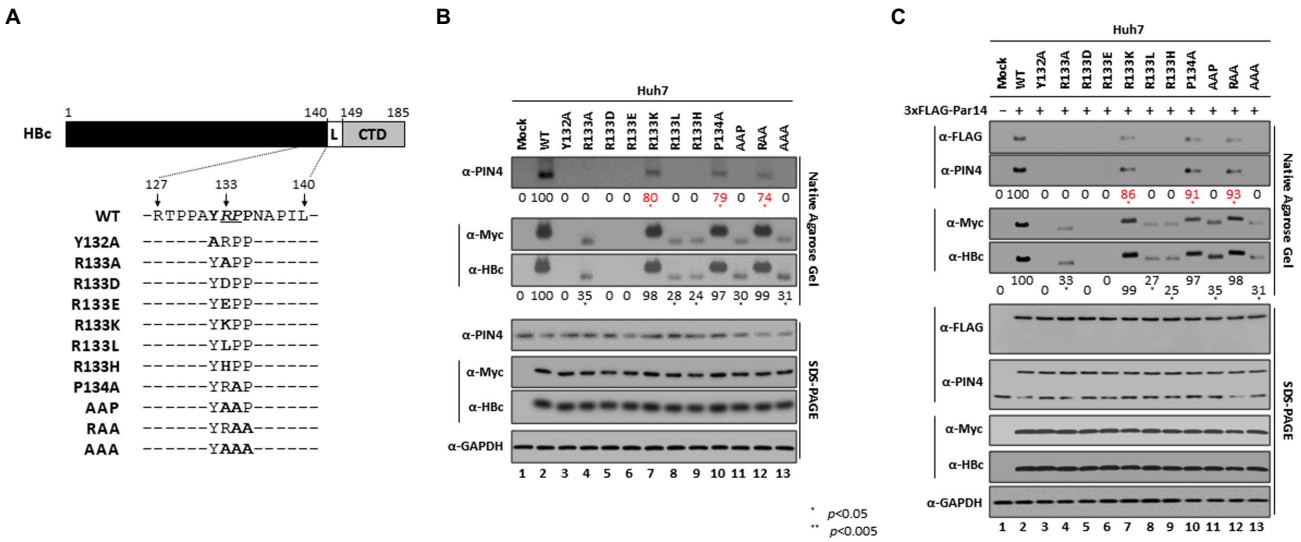

FIGURE 4 | The positively charged R133 residue in the conserved RP motif is critical for core particle assembly and interactions with Par14/Par17. **(A)** Schematic diagram of the HBc protein. The HBc ^{132}YRPP^{135} motif and single, double, and triple YRPP substitution mutants are indicated. **(B,C)** The positively charged R133 residue in the conserved RP motif is critical for core particle assembly and interactions with Par14/Par17. Huh7 cells in 6 cm plates were mock-transfected (lane 1) or transfected with Myc-HBc WT (lane 2), Myc-HBc-Y132A (lane 3), or Myc-HBc RP motif mutants (lanes 4–13) **(B)**. Huh7 cells were mock-transfected (lane 1) or co-transfected with 3 × FLAG-Par14 WT plus Myc-HBc WT (lane 2), Myc-HBc-Y132A (lane 3), or Myc-HBc RP motif mutants (lanes 4–13). At 72 h post-transfection, lysates were prepared and subjected to NAGE plus immunoblotting and SDS-PAGE plus immunoblotting, as described in **Figure 1**. Relative levels of Par14/Par17 bound to core particles and of core particles were calculated using ImageJ v.1.46r. Representative data from three independent experiments are shown. Statistical significance was evaluated using Student's *t*-test. $^{*}p < 0.05$ relative to the corresponding control.

HBc protein has an additionally conserved KP motif (**Figure 3C**).

The Positively Charged R133 Residue in the Conserved RP Motif Is Critical for Core Particle Assembly and Interactions With Par14/Par17

To investigate the importance of the HBc RP motif, several RP motif mutants were constructed (**Figure 4A**) and core particle assembly was examined (**Figure 4B**, second and third panels). Expression of all HBc mutant proteins was comparable with that of HBc WT (**Figure 4B**, fifth and sixth panels). NAGE and immunoblotting revealed that a comparable level of core particles was assembled with the HBc-R133K, -P134A, and -RAA mutants as with HBc WT (**Figure 4B**, second and third panels, lanes 2 vs. 7, 10, and 12), indicating that a R or K residue at position 133 is critical for core particle assembly, but P134 and P135 are not. When R133 was changed to a D or E residue, the HBc mutant proteins showed an assembly-defective phenotype similar to HBc-Y132A (**Figure 4B**, second and third panels, lanes 3 vs. 5 and 6), suggesting that a negatively charged residue at position 133 interferes with core particle assembly, supposedly like HBc-Y132A (Bourne et al., 2009). Although other RP motif mutants (HBc-R133A, -R133L, -R133H, -AAP, and -AAA) were core particle assembly-positive with a reduced efficiency (**Figure 4B**, second and third panels, lanes 2 vs. 4, 8, 9, 11, and 13), endogenous Par14/Par17 could not bind to these mutant core particles (**Figure 4B**, top panel), indicating that a R or K at position 133 is critical for Par14/Par17 binding. Consistently, Par14/Par17 bound to core particles assembled by HBc-R133K, -P134A, and -RAA (**Figure 4B**, top panel, lanes 2 vs. 7, 10, and 12), further strengthening the above conclusion. Our results indicate that core particle–Par14/Par17 interactions stabilize the core particle or improve the efficiency of its assembly (**Figure 4B**, second and third panels, lanes 2, 7, 10, and 12 vs. 4, 8, 9, 11, and 13). Of note, core particles assembled by HBc-R133A, −R133L, -R133H, -AAP, and -AAA migrated rapidly in the agarose gel (**Figure 4B**, second and third panels, lanes 2 vs. 4, 8, 9, 11, and 13).

In Par14- or Par17-overexpressing cells, core particle assembly, core particle migration in the agarose gel, and core particle–Par14/Par17 interactions were all identical with **Figure 4B** (**Figure 4C** and **Supplementary Figure S3**). Core particles were not detected in the nucleus (**Supplementary Figure S4**), demonstrating that core particle–Par14/Par17 interactions must occur in the cytoplasm, not in the nucleus.

Unlike Core Particle Assembly-Defective HBc-Y132A, Core Particle Assembly-Defective HBc-R133D and -R133E Cannot Interact With Par14/Par17

The HBc-R133D and -R133E mutants were core particle assembly-defective similar to HBc-Y132A (**Supplementary Figures 4B,C**, and **Figure 5A**, eighteenth and bottom panels, lanes 2 vs. 3, 4 and 5). Therefore, we examined HBc–Par14/Par17 interactions. Although HBc-Y132A interacted with Par14/

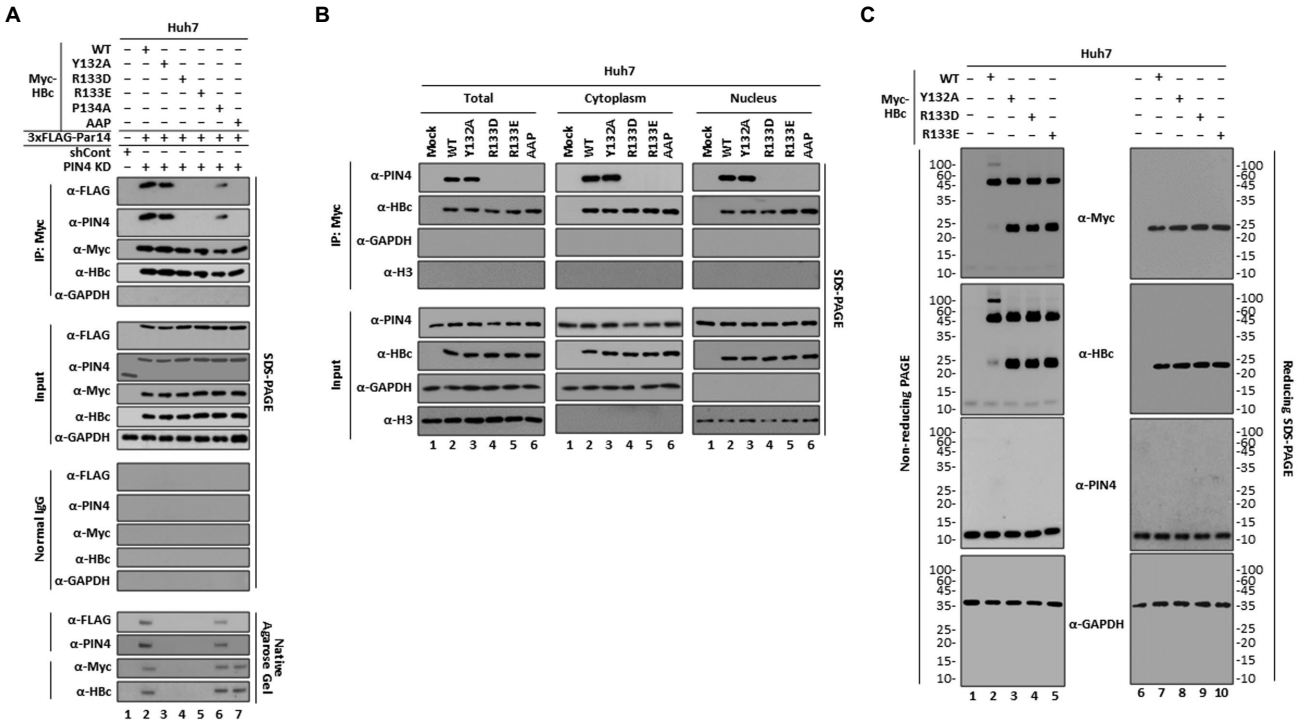

FIGURE 5 | Unlike core particle assembly-defective HBc-Y132A, core particle assembly-defective HBc-R133D and -R133E cannot interact with Par14/Par17. **(A)** The HBc ^{133}RP^{134} motif is important for binding to Par14. *PIN4*-KD Huh7 cells in 6 cm plates were co-transfected with 3 × FLAG-Par14 WT plus Myc-HBc WT (lane 2), -Y132A (lane 3), -R133D (lane 4), −R133E (lane 5), -P134A (lane 6), or -AAP (lane 7). Control shRNA-transduced and mock-transfected Huh7 cells were used as a negative control (lane 1). Lysates were immunoprecipitated with an anti-Myc antibody and immunoblotted with an anti-FLAG antibody. Lysates were subjected to NAGE and SDS-PAGE and then immunoblotted with anti-FLAG, anti-PIN4, anti-Myc, anti-HBc, and anti-GAPDH antibodies, as described in **Figure 1**. **(B)** Endogenous Par14/Par17 can interact with HBc WT and -Y132A in the nucleus and cytoplasm, unlike HBc-R133D, −R133E, and -AAP. Huh7 cells were mock-transfected (lane 1) or transfected with Myc-HBc WT (lane 2), -Y132A (lane 3), -R133D (lane 4), −R133E (lane 5), or -AAP (lane 6). At 72 h post-transfection, total cell lysates and cytoplasmic and nuclear fractions were prepared and analyzed by SDS-PAGE and immunoblotting [35]. **(C)** HBc-R133D and HBc-R133E may form dimers, similar to HBc-Y132A. Huh7 cells were mock-transfected (lanes 1 and 6) or transfected with Myc-HBc WT (lanes 2 and 7), -Y132A (lanes 3 and 8), -R133D (lanes 4 and 9), or -R133E (lanes 5 and 10). At 72 h post-transfection, whole-cell lysates were prepared and subjected to non-reducing PAGE or reducing SDS-PAGE as described in the "Materials and Methods" section, and then immunoblotted with anti-Myc, anti-HBc, anti-PIN4, and anti-GAPDH antibodies. Representative data from three independent experiments are shown.

Par17 similar to HBc WT (**Figures 1D**, **5A**, and **Supplementary Figure S5**, top and second panels, lane 2 vs. 3), the HBc-R133D, -R133E, and -AAP mutants did not interact with Par14/Par17 (**Figure 5A** and **Supplementary Figure S5**, top and second panels, lanes 2 and 3 vs. 4, 5, and 7) and HBc-P134A interacted with Par14/Par17 with a reduced efficiency (**Figure 5A** and **Supplementary Figure S5**, top and second panels, lanes 2 and 3 vs. 6). These results further demonstrate that R133 is critical for HBc–Par14/Par17 interactions.

Next, we investigated HBc–Par14/Par17 interactions in total, cytoplasmic, and nuclear fractions (**Figure 5B**). While HBc WT and -Y132A strongly interacted with endogenous Par14/Par17 in the total, cytoplasmic, and nuclear fractions, HBc-R133D, −R133E, and -AAP did not interact with Par14/Par17 at all (**Figure 5B**), further demonstrating the importance of R133 in ^{133}RP^{134} motif for Par14/Par17 binding.

Par14/Par17 facilitate the nuclear localization of HBx *via* its RP motifs (Saeed et al., 2019); therefore, we investigated whether binding of Par14/Par17 to HBc *via* the RP motif also affects its intracellular localization. Consistent with the previously reported localization of HBc *in vivo* (Diab et al., 2018),HBc WT and HBc RP motif mutants were detected both in the cytoplasm and nucleus (**Supplementary Figure S4**). However, we did not detect core particles in the nucleus by NAGE (**Supplementary Figure S4**). Unlike HBx (Saeed et al., 2019), Par14 WT did not affect the nuclear or cytoplasmic localization of HBc WT or mutants (**Supplementary Figure S6A**). The same results were obtained upon co-transfection of Par17 WT (**Supplementary Figure S6B**).

The dimer-positive HBc-Y132A mutant cannot assemble into core particles due to a deficiency of interdimeric interactions (Bourne et al., 2009). Therefore, we investigated whether core particle assembly-defective HBc-R133D or -R133E can form dimers similar to HBc-Y132A. Cytoplasmic lysates were subjected to non-reducing PAGE or conventional reducing SDS-PAGE and immunoblotting (**Figure 5C**). Consistent with the above results (**Figures 4B,C** and **5A,B**), expression levels of HBc proteins were comparable under reducing conditions (**Figure 5C**, lanes 7–10). Under non-reducing conditions, HBc WT formed a high molecular weight complex of HBc and dimeric HBc,

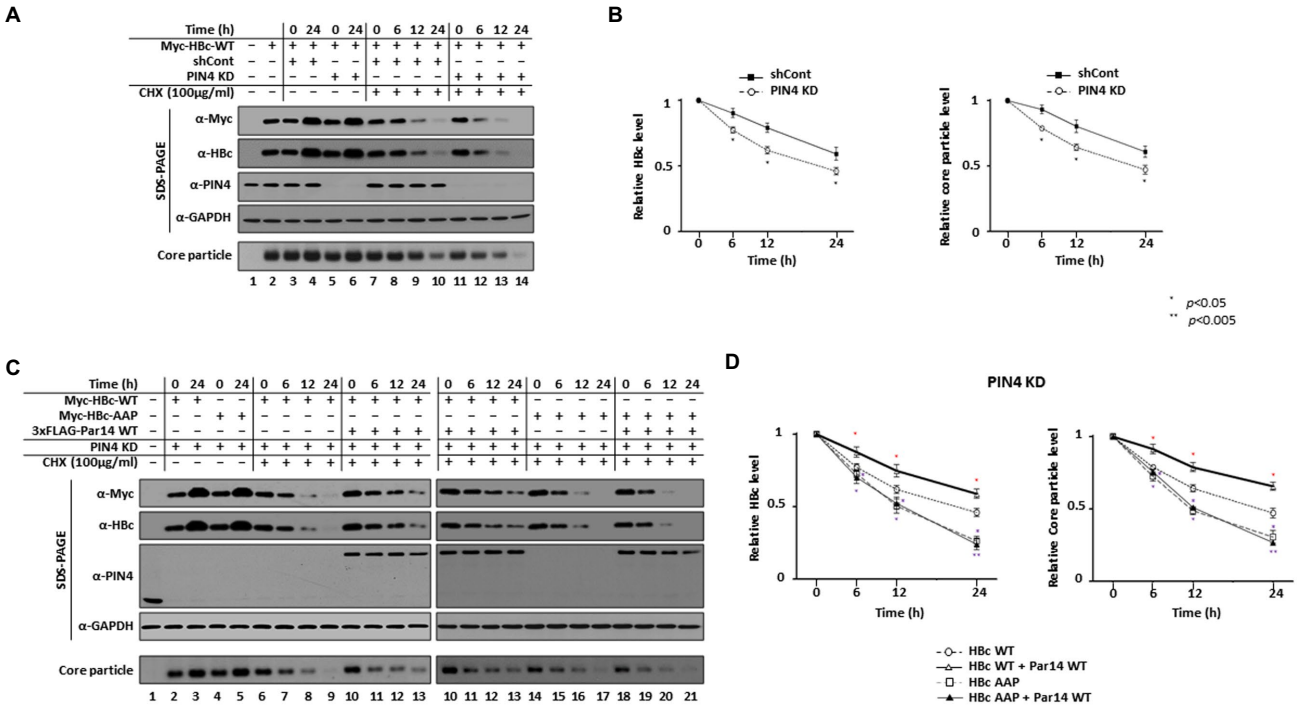

FIGURE 6 | Par14/Par17 can stabilize both HBc and the core particle through their interactions *via* the HBc RP motif. **(A,B)** The stabilities of HBc and the core particle are decreased in *PIN4*-KD Huh7 stable cells. Control shRNA-transduced (lanes 3, 4, and 7–10) and *PIN4*-KD (lanes 5, 6, and 11–14) Huh7 cells were transfected with Myc-HBc WT (lanes 2–14). As controls, Huh7 cells were mock-transfected (lane 1) or transfected with Myc-HBc WT (lane 2). At 24 h post-transfection, cells were treated with DMSO (lanes 2–6) or 100 μg/ml cycloheximide diluted in DMSO (lanes 7–14) and lysates were prepared at the indicated time points. **(C,D)** Par14 increases the stabilities of HBc and the core particle through the HBc ^{133}RP^{134} motif. *PIN4*-KD Huh7 cells (lanes 2–21) were transfected with Myc-HBc WT (lanes 2, 3, and 6–9) or Myc-HBc-AAP (lanes 4, 5, and 14–17) or co-transfected with 3 × FLAG-Par14 WT plus Myc-HBc WT (lanes 10–13) or Myc-HBc-AAP (lanes 18–21). Mock-transfected Huh7 cells were used as a negative control (lane 1). At 24 h post-transfection, cycloheximide-treated cells generated as described above were harvested at the indicated time points and subjected to SDS-PAGE and NAGE followed by immunoblotting with anti-Myc, anti-HBc, anti-PIN4, and anti-GAPDH antibodies. Representative results from three independent experiments are shown. Data are presented as mean HBc and core particle levels ± SD. Statistical significance was evaluated using Student's *t*-test. *$p < 0.05$ relative to the corresponding control.

with a very low level of monomeric HBc (**Figure 5C**, lane 2). However, HBc-Y132A, -R133D, and -R133E formed a comparable level of dimeric HBc as HBc WT and much higher levels of monomeric HBc than HBc WT, and did not form a high molecular weight complex of HBc (**Figure 5C**, lanes 2 vs. 3, 4, and 5), suggesting that dimeric HBc-R133D and -R133E are defective in core particle assembly due to a deficiency of interdimeric interactions similar to HBc-Y132A.

Par14/Par17 Stabilize Both HBc and the Core Particle Through Their Interactions *via* the HBc RP Motif

Par14 and Par17 interact with and thereby stabilize HBx (Saeed et al., 2019); therefore, we reasoned that they may also stabilize HBc and/or the core particle through their interactions even though HBc and/or the core particle are relatively stable. In *PIN4*-KD cells, the levels of HBc and core particles were decreased after 6 h and these decreases were enhanced after 12 h and peaked after 24 h compared with control cells (**Figure 6A**, top, second, and bottom panels, lanes 7–10 vs. 11–14). Accordingly, the half-lives of HBc (**Figure 6B** left) and the core particle (**Figure 6B** right) were decreased from >24 to 20 h and from >24to 21 h, respectively (**Figure 6B**).

When we exogenously expressed Par14 WT (**Figures 6C,D**) or Par17 WT (**Supplementary Figure S7**) in *PIN4*-KD cells, the half-lives of HBc and the core particle were increased from 20 to >24 h and from 21 to >24 h, respectively (**Figure 6D** left and Supplementary Figure S7), demonstrating that Par14 or Par17 increase the stabilities of HBc and the core particle (**Figures 6C** and **Supplementary Figure S7**, lanes 6–9 vs. 10–13). The half-life of HBc, which decreased from >24 to 20 h in *PIN4*-KD Huh7 cells, was further decreased from 20 to 12 h upon RP motif mutation (HBc-AAP). Likewise, the half-life of the core particle, which decreased from >24 to 21 h in *PIN4*-KD Huh7 cells, was further decreased to 13 h upon RP motif mutation (HBc-AAP), which clearly demonstrates the importance of the RP motif for stability of HBc. Unlike HBc WT, the presence or absence of Par14/Par17 did not affect the levels of HBc-AAP or core particles formed by HBc-AAP (**Figure 6C**, lanes 6–9 vs. 10–13 vs. 14–17 vs. 18–21, and **Supplementary Figure S7**). Furthermore, Par14 WT and Par 17 WT did not change the half-life of HBc-AAP or core particles formed by HBc-AAP (**Figure 6D**

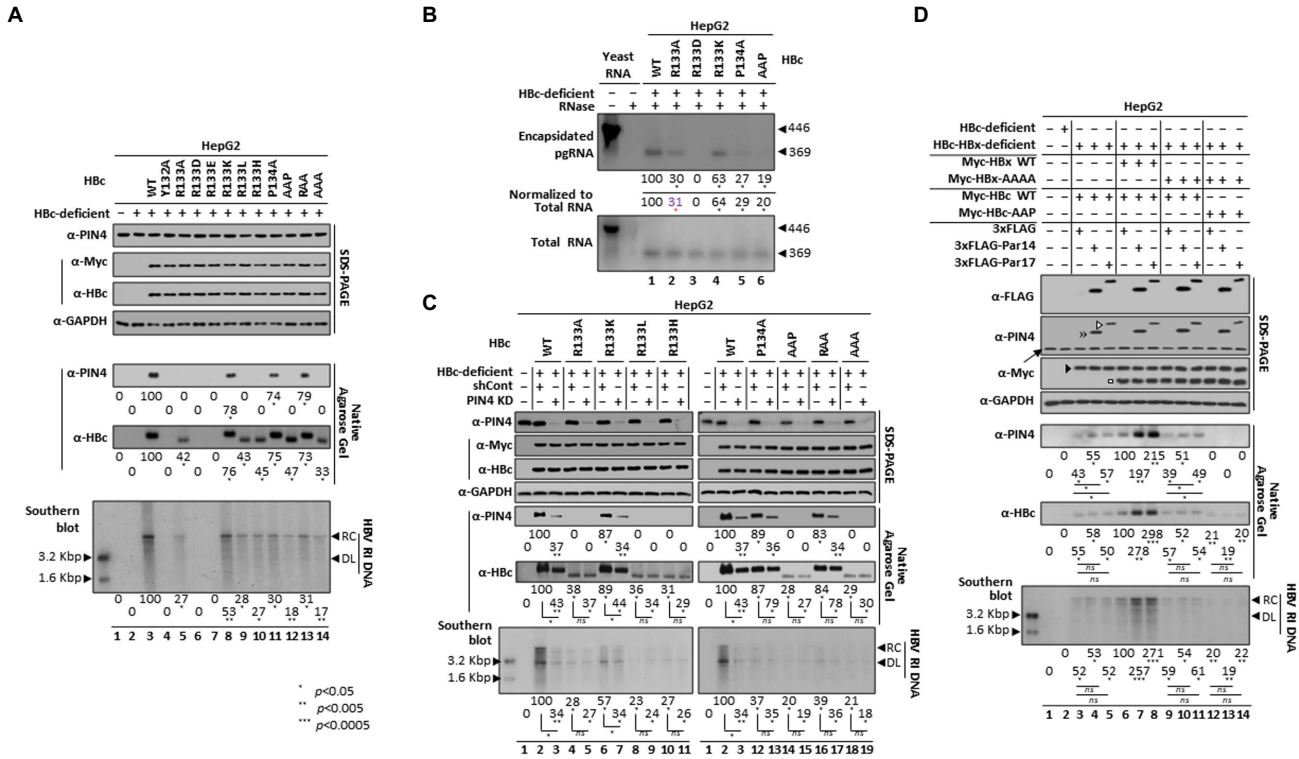

FIGURE 7 | The HBc RP motif is critical for Par14/Par17-mediated upregulation of HBV replication. **(A)** HBc RP motif mutants impair HBV replication. HepG2 cells in 6 cm plates were mock-transfected (lane 1), transfected with HBc-deficient HBV (lane 2), or co-transfected with HBc-deficient HBV plus Myc-HBc WT (lane 3), Myc-HBc-Y132A (lane 4), or Myc-HBc RP motif mutants (lanes 5–14). **(B)** The HBc RP motif is critical for pgRNA encapsidation. To examine encapsidated pgRNA and total RNA from HepG2 cells co-transfected with HBc-deficient HBV plus Myc-HBc WT or HBc RP motif mutants, an *in vitro*-transcribed DIG-UTP-labeled antisense RNA probe (446 nt) was hybridized overnight at 50°C with pgRNA from isolated core particles or 10 μg of total RNA. Protected RNA (369 nt) following RNase digestion was electrophoresed on a 5% polyacrylamide–8 M urea gel, transferred to a nylon membrane (Roche, Sigma-Aldrich #11417240001), immunoblotted with an anti-DIG-AP antibody, and visualized with CSPD. **(C)** The positively charged R133 or K133 residue in the RP motif facilitates core particle assembly, resulting in efficient HBV replication. Control shRNA-transduced (lanes 2, 4, 6, 8, 10, 12, 14, 16, and 18) and stable *PIN4*-KD (lanes 3, 5, 7, 9, 11, 13, 15, 17, and 19) cells were co-transfected with HBc-deficient HBV plus Myc-HBc WT (lanes 2 and 3) or Myc-HBc RP motif mutants (lanes 4–19). **(D)** Both HBx ^{19}RP^{20}-^{28}RP^{29} motifs and the HBc ^{133}RP^{134} motif are critical for Par14/Par17-mediated upregulation of HBV replication. HepG2 cells were mock-transfected (lane 1) or transfected with HBc-deficient HBV (lane 2). HepG2 cells were triple-transfected with HBc-HBx-deficient HBV plus Myc-HBc WT plus 3 × FLAG (lane 3), 3 × FLAG-Par14 WT (lane 4), or 3 × FLAG-Par17 WT (lane 5). HepG2 cells were quadruple-transfected with HBc-HBx-deficient HBV plus Myc-HBc WT plus Myc-HBx WT plus 3 × FLAG (lane 6), 3 × FLAG-Par14 WT (lane 7), or 3 × FLAG-Par17 WT (lane 8). HepG2 cells were quadruple-transfected with HBc-HBx-deficient HBV plus Myc-HBc WT plus Myc-HBx-AAAA plus 3 × FLAG (lane 9), 3 × FLAG-Par14 WT (lane 10), or 3 × FLAG-Par17 WT (lane 11). HepG2 cells were quadruple-transfected with HBc-HBx-deficient HBV plus Myc-HBc-AAP plus Myc-HBx-AAAA plus 3 × FLAG (lane 12), 3 × FLAG-Par14 WT (lane 13), or 3 × FLAG-Par17 WT (lane 14). The amount of transfected DNA was adjusted with the pCMV empty vector. Lysates were prepared at 72 h post-transfection and subjected to SDS-PAGE and NAGE, as described in **Figure 1**. Overexpressed Myc-tagged HBc and Myc-tagged HBx are marked by a closed arrowhead and open square, respectively (**D**, third panel). Southern blotting detected HBV replicative intermediate, partially double-stranded RC, and double-stranded linear DNAs, marked as HBV RI DNA, RC, and DL, respectively. The levels of the HBV core particle, Par14/Par17-binding to the core particle, and HBV DNA was measured using ImageJ v.1.46r. Representative results from three independent experiments are shown. Statistical significance was evaluated using Student's *t*-test. $^{*}p < 0.05$, $^{**}p < 0.005$, and $^{***}p < 0.0005$ relative to the corresponding control.

and **Supplementary Figure S7**). The overall levels of HBc-AAP and core particles formed by HBc-AAP were always less than in control cells (**Figure 6C**, lanes 6–9 vs. 10–13 vs. 14–17 vs. 18–21), indicating that HBc-AAP and core particles formed by HBc-AAP cannot be stabilized due to the lack of Par14/Par17 interactions. Of note, Par14/Par17 increased the stability of HBc-Y132A, but not of HBc-R133D (**Supplementary Figure S8**). Taken together, we reasoned that HBc and the core particle are stabilized through specific HBc– and/or core particle–Par14/Par17 interactions.

The HBc RP Motif Is Crucial for Par14/Par17-Mediated Upregulation of HBV Replication

In light of our observation that the HBc ^{133}RP^{134} motif is important for HBc– and/or core particle–Par14/Par17 interactions (**Figures 4, 5**) and that Par14/Par17 upregulate HBV replication in an HBx-dependent manner (Saeed et al., 2019), we speculated that HBc– and/or core particle–Par14/Par17 interactions may also be involved in HBV replication. In accordance with **Figure 4**, the expression levels of proteins, core particle assemblies, core particle migration patterns, and core particle–Par14/Par17

interactions were presented (**Figure 7A**). As expected, HBc-Y132A, -R133D, and -R133E were replication-defective (**Figure 7A**, bottom panel, lanes 4, 6, and 7). HBc-R133A, -R133L, -R133H, -AAP, and -AAA supported HBV replication with a reduced efficiency (**Figure 7A**, bottom panel, lanes 5, 9, 10, 12, and 14) and were deficient in core particle–Par14/Par17 interactions (fifth panel). Although core particles formed by HBc-R133K, -P134A, and -RAA interacted with Par14/Par17 with similar efficiencies (**Figure 7A**, fifth and sixth panels, lanes 8, 11, and 13), HBV DNA synthesis was higher with HBc-R133K than with HBc-P134A and -RAA (**Figure 7A**, bottom panel, lanes 8 vs. 11 and 13). HBV DNA synthesis with HBc-P134A and -RAA was similar to that with HBc-R133A, -R133L, and -R133H (**Figure 7A**, bottom panel, lanes 11 and 13 vs. 5, 9, and 10), indicating that the RP motif itself is important for HBV replication. HBV replication with HBc-R133K was 53% of that with HBc WT, indicating that the RP motif is preferable to the KP motif for HBV replication (**Figure 7A**, bottom panel, lanes 3 vs. 8). HBV DNA synthesis was reduced more by HBc-AAP than by other core particle assembly-competent HBc RP mutants (**Figure 7A**, bottom panel, lanes 5, 8–11, and 13 vs. 12). HBV replication with HBc-AAA was comparable to that with HBc-AAP, demonstrating that P135 is not important for HBV replication (**Figure 7A**, bottom panel, lane 12 vs. 14).

Core particle assembly and HBV DNA synthesis were reduced by HBc RP motif mutants; therefore, pgRNA encapsidation from isolated core particles was examined by the RPA (**Figure 7B**). Except for the core particle assembly-defective HBc-R133D (**Figure 7B**, lane 3), the selected HBc RP mutants could encapsidate pgRNA with reduced efficiencies (**Figure 7B**, lanes 1 vs. 2 and 4–6). In accordance with HBV DNA synthesis (**Figure 7A**, bottom panel, lanes 3 vs. 8), pgRNA encapsidation by HBc-R133K was 63% of that by HBc WT (**Figure 7B**, lane 1 vs. 4). The decreased level of pgRNA encapsidated by HBc-AAP (**Figure 7B**, lane 1 vs. 6) was also comparable with the level of HBV DNA synthesis (**Figure 7A**, bottom panel, lanes 3 vs. 12), demonstrating that the RP motif is critical for pgRNA encapsidation.

Next, core particle assembly, core particle–Par14/Par17 interactions, and HBV DNA synthesis were compared between control and *PIN4*-KD HepG2 cells (**Figure 7C**). Core particle assembly by HBc WT and HBc-R133K was reduced in *PIN4*-KD cells (**Figure 7C**, sixth panel, lanes 2 vs. 3 and 6 vs. 7). However, core particle assembly by other HBc RP mutants was not reduced (**Figure 7D**, sixth panel), indicating that efficient core particle assembly is facilitated by a positively charged R or K residue in the RP motif. In accordance with the above results (**Figures 4B,C**, top panels, and **Figure 7A**, fifth panel), core particle–Par14/Par17 interactions with HBc WT, HBc-R133K, -P134A, and -RAA were presented (**Figure 7D**, fifth panel). As expected, core particle–Par14/Par17 interactions with these HBc proteins were decreased in *PIN4*-KD cells (**Figure 7D**, fifth panel). Consistent with core particle assembly by HBc WT and HBc-R133K (**Figure 7D**, sixth panel, lanes 2 vs. 3 and 6 vs. 7), HBV DNA synthesis was reduced in *PIN4*-KD cells (**Figure 7D**, bottom panel, lanes 2 vs. 3 and 6 vs. 7), in contrast with the other RP mutants. HBV DNA synthesis was decreased more with HBc WT than with HBc-R133K in *PIN4*-KD cells, indicating that RP is more preferred than KP for Par14/Par17 effects. When Par14 or Par17 was overexpressed, HBV replication was only enhanced with HBc WT and HBc-R133K (S10 and S11 Figs), further strengthening the importance of the RP or KP motif.

Par14/Par17 enhance HBV replication in an HBx-dependent manner by binding to the ^{19}RP^{20} and ^{28}RP^{29} motifs of HBx (Saeed et al., 2019). Therefore, Par14/Par17-mediated replication of HBc-HBx-double-deficient HBV was investigated. As expected, when HBc WT plus HBx WT were supplied to double-deficient HBV, Par14 WT and Par17 WT enhanced HBV replication (**Figure 7D**, sixth and bottom panels, lanes 6–8). When HBc WT was supplied to double-deficient HBV, neither Par14 WT nor Par17 WT enhanced HBV replication (**Figure 7D**, sixth and bottom panels, lanes 3–5), demonstrating the requirement for HBx (Saeed et al., 2019). When HBc WT plus HBx-AAAA were supplied, neither Par14 WT nor Par17 WT enhanced HBV replication, similar to cells that were only supplied HBc WT (**Figure 7D**, sixth and bottom panels, lanes 3–5 vs. 9–11). When HBc-AAP plus HBx-AAAA were supplied, HBV replication was not enhanced by Par14 WT or Par17 WT and was the lowest among the examined cells (**Figure 7D**, sixth and bottom panels, lanes 3–5, 6–8, 9–11, vs. 12–14), indicating that specific HBx–Par14/Par17 interactions and specific HBc– and/or core particle–Par14/Par17 interactions upregulate HBV replication.

The HBc RP Motif Is Crucial for Par14/Par17-Mediated HBV Replication in an Infection System

To substantiate the aforementioned findings in an HBV infection system, virions of the full-length subtype adwR9 HBV WT (Kim et al., 2004) and the corresponding HBV-HBc-AAP mutant were prepared from transfected HepG2 cells. pgRNA transcription was controlled by the CMV IE promoter. To infect HepG2-hNTCP-C9 cells, the HBV WT or mutant HBV-HBc-AAP virion inoculum was adjusted to approximately 1.7×10^3 genome equivalents (GEq) per cell. Of note, while preparing HBV virions, mutant HBV-HBc-AAP produced 7 times less viruses than HBV WT (0.55×10^7 GEq/ml vs. 3.87×10^7 GEq/ml), further indicating that the RP motif is crucial for viral replication. The levels of HBV RNAs, HBc protein, core particle assembly, core particle–Par14/Par17 interactions, and HBV DNA synthesis were lower in HBV-HBc-AAP-infected cells than in HBV WT-infected cells (**Figure 8A**, third, sixth, eighth, ninth, and bottom panels, lane 2 vs. 3). However, the level of cccDNA was comparable (**Figure 8A**, fifth panel, lane 2 vs. 3).

Next, shControl and *PIN4*-KD-HepG2-hNTCP-C9 cells were infected with HBV WT or mutant HBV-HBc-AAP. Consistent with **Figure 8A**, infection of shControl cells generated the same results (**Figure 8B**, third, fifth, sixth, ninth, and bottom panels, lane 2 vs. 3). As expected, the levels of HBV RNAs, HBc protein, core particle assembly, and HBV DNA synthesis

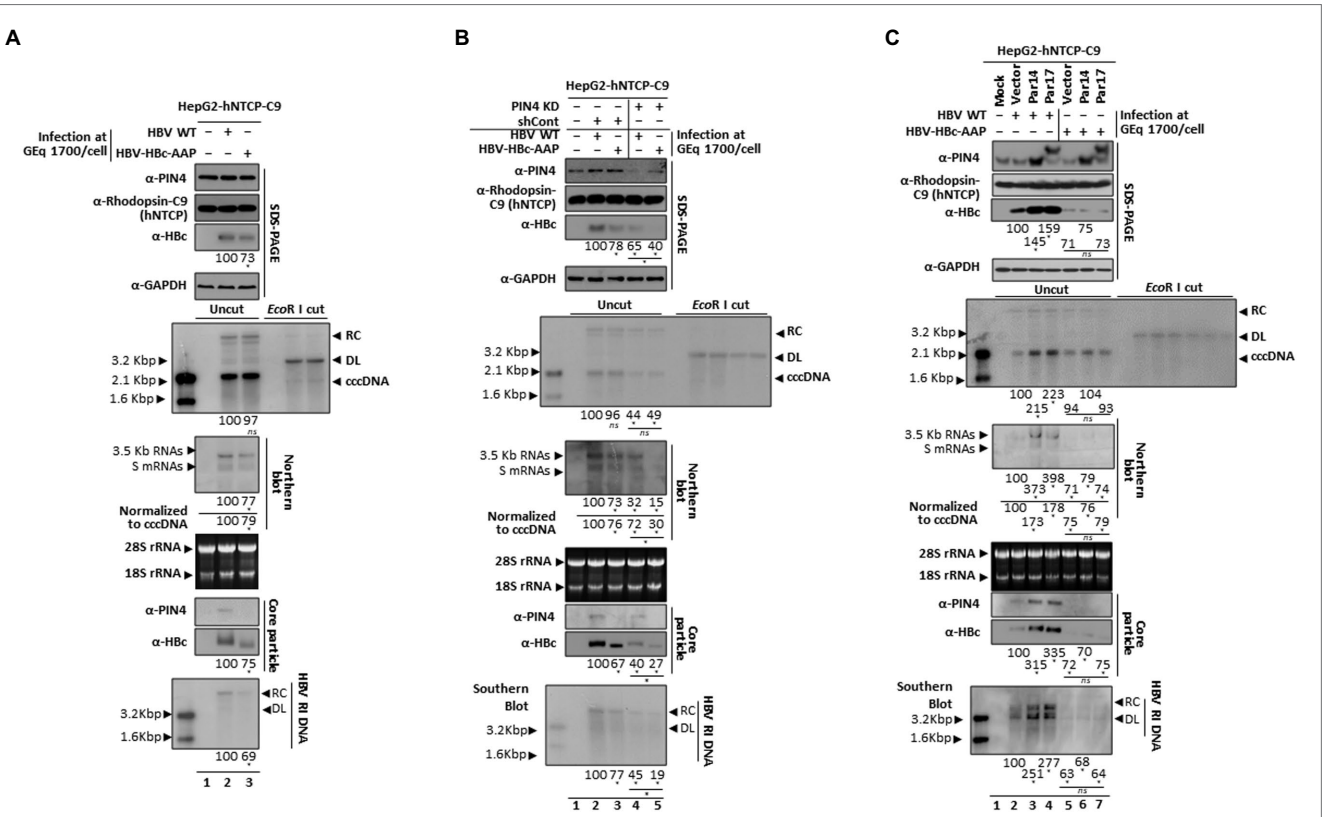

FIGURE 8 | The HBc RP motif is critical for Par14/Par17-mediated HBV replication in infected cells. **(A)** HBV replication was significantly decreased with HBV-HBc-AAP, demonstrating that the HBc ^{133}RP^{134} motif is important. A total of 2×10^5 HepG2-hNTCP-C9 cells were grown in collagen-coated 6-well plates, infected with 1.7×10^3 GEq of HBV WT (lane 2) or HBV-HBc-AAP mutant (lane 3) virions as described in the "Materials and Methods" section, and lysed at 9 days p.i. Lane 1 is a mock-infected control. **(B)** Decreased HBV replication in *PIN4* KD cells was further inhibited upon HBV-HBc-AAP infection. HepG2-hNTCP-C9-shControl (lanes 2 and 3) and HepG2-hNTCP-C9-shPIN4-#5 (lanes 4 and 5) cells were infected with HBV WT and HBV-HBc-AAP mutant virions, as described above. Lane 1 is mock-infected control HepG2-hNTCP-C9 cells. **(C)** Although Par14 and Par17 overexpression increased HBV replication in HBV WT-infected cells, it did not affect HBV replication in HBV-HBc-AAP-infected cells. Mock- (lane 1), empty vector- (lanes 2 and 5), Par14- (lanes 3 and 6), and Par17-transduced (lanes 4 and 7) HepG2-hNTCP-C9 cells were infected with 1.7×10^3 GEq of HBV WT (lane 2–4) or HBV-HBc-AAP mutant (lanes 5–7) virions and lysed at 5 (for total RNA) or 9 days p.i. HBV cccDNA was extracted and subjected to Southern blotting as described previously [35]. For Northern blotting, 20 μg of total RNA was loaded per lane. The 3.5 kb pgRNA, 2.1 and 2.4 kb S mRNAs, and 28S and 18S ribosomal RNAs are indicated. SDS-PAGE and immunoblotting, NAGE and immunoblotting of core particles, and Southern blotting were performed as described above. Relative levels of core particles, HBV RNAs, HBV cccDNA, and HBV RI DNAs were measured using ImageJ v.1.46r. Viral RNA levels were normalized to cccDNA levels. Data are presented as means from three independent experiments. Statistical significance was evaluated using Student's *t*-test. $^*p < 0.05$ relative to the corresponding control.

were lower in HBV-HBc-AAP-infected *PIN4*-KD cells than in HBV WT-infected *PIN4*-KD cells (**Figure 8B**, third, sixth, ninth, and bottom panels, lane 4 vs. 5). However, the ratio was more drastic in *PIN4*-KD cells (**Figure 8B**, lanes 2 vs. 3; lanes 4 vs. 5). The cccDNA level was comparable (**Figure 8B**, fifth panel, lane 4 vs. 5).

In HBV WT-infected, Par14/Par17-overexpressing cells, HBV cccDNA, HBV RNAs, HBc protein, core particle assembly, core particle–Par14/Par17 interactions, and HBV DNA synthesis were all significantly increased (**Figure 8C**, third, fifth, sixth, eighth, ninth, and bottom panels, lanes 2 vs. 3 and 4). However, HBV-HBc-AAP infection of Par14- or Par17-overexpressing HepG2-hNTCP-C9 cells did not affect HBV replication at all (**Figure 8C**, lanes 5 vs. 6 and 7), demonstrating that the RP motif of HBc is critical for Par14/Par17-mediated upregulation of HBV replication.

Par14/Par17 Promote Recruitment of HBc Into HBV cccDNA in the Nucleus

HBV nuclear cccDNA is organized as a minichromosome in association with histone and non-histone cellular and viral proteins, including viral HBx and HBc proteins (Bock et al., 2001; Lucifora and Protzer, 2016; Piracha et al., 2020). We previously demonstrated HBx–Par14/Par17–cccDNA interactions in the nucleus (Saeed et al., 2019).

HBc associates with cccDNA as a non-histone protein (Bock et al., 2001; Guo et al., 2011; Lucifora and Protzer, 2016; Diab et al., 2018; Piracha et al., 2020) and HBc-Par14/Par17 interactions (**Figures 1, 2**, and **5A,B**) were also detected in the nucleus (**Figure 5B**). Therefore, recruitment of HBc onto cccDNA in the presence or absence of Par14/Par17 was examined by ChIP. Consistent with the previous report, Par14/Par17 overexpression enhanced recruitment of RNA polymerase II and acetylated

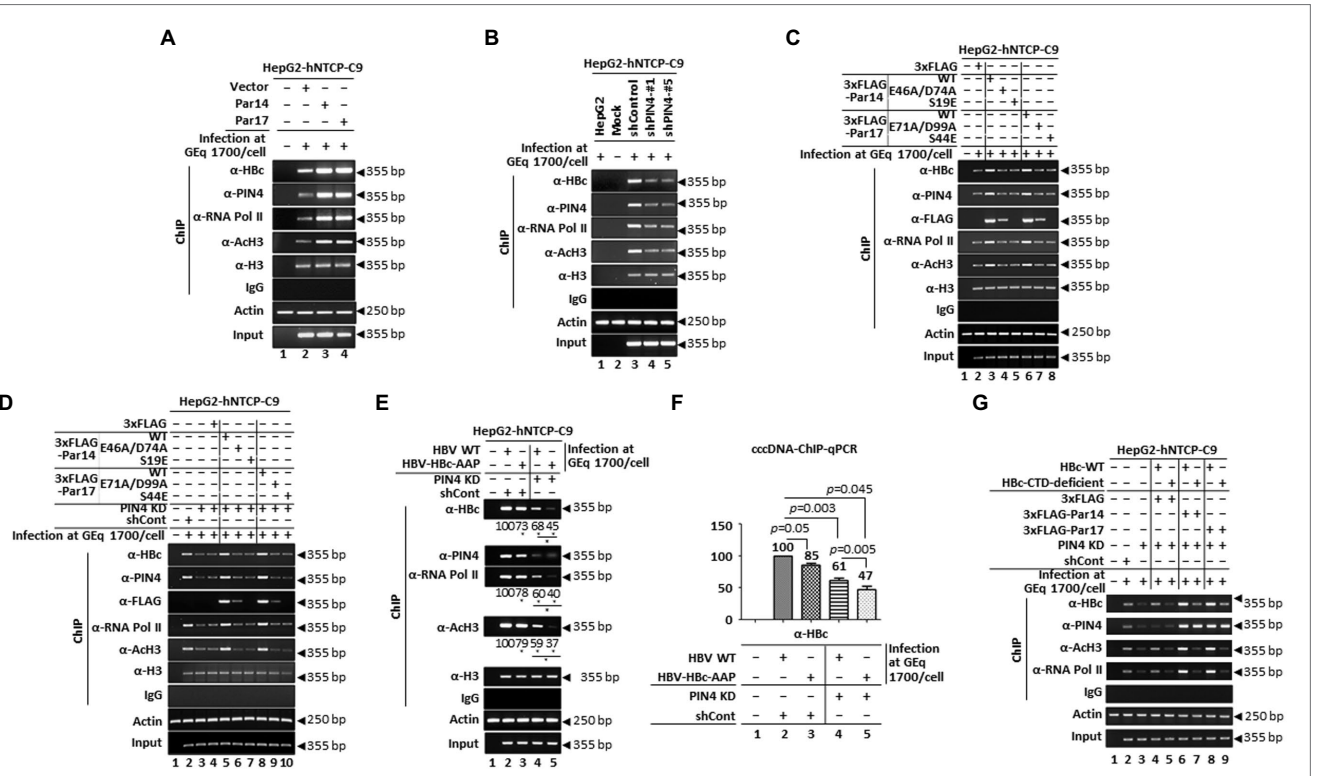

FIGURE 9 | The S19 and E46/D74 residues of Par14 and S44 and E71/D99 residues of Par17 promote recruitment of HBc into cccDNA *via* the HBc RP motif. **(A)** Overexpressed Par14 and Par17 increase recruitment of HBc into cccDNA. Vector- (lane 2), Par14- (lane 3), and Par17-transduced (lane 4) HepG2-hNTCP-C9 cells were infected with 1.7×10^3 GEq of HBV WT. Mock-infected HepG2-hNTCP-C9 cells were used a negative control (lane 1). **(B)** *PIN4* KD reduces binding of HBc to cccDNA. HepG2-hNTCP-C9-shControl (lane 3), HepG2-hNTCP-C9-shPIN4-#1 (lane 4), and HepG2-hNTCP-C9-shPIN4-#5 (lane 5) cells were infected with HBV as described above. HepG2 cells were infected (lane 1) and HepG2-hNTCP cells were mock-infected (lane 2) as negative controls. **(C,D)** Substrate- and DNA-binding residues of Par14 (E46/D74 and S19, respectively) and Par17 (E71/D99 and S44, respectively) are important for enhanced recruitment of HBc into cccDNA. HepG2-hNTCP-C9 cells were plated as described above and mock-transfected (lane 1) or transfected with 3 × FLAG (lane 2), 3 × FLAG-Par14 WT (lane 3), 3 × FLAG-Par14-E46A/D74A (lane 4), 3 × FLAG-Par14-S19E (lane 5), 3 × FLAG-Par17 WT (lane 6), 3 × FLAG-Par17-E71A/D99A (lane 7), or 3 × FLAG-Par17-S44E (lane 8) **(C)**. HepG2-hNTCP-C9 (lane 1), HepG2-hNTCP-C9-shControl (lane 2), and HepG2-hNTCP-C9-shPIN4-#1 (lanes 3–10) cells were seeded as described above. As additional controls, HepG2-hNTCP-C9-shPIN4-#1 cells were mock-transfected (lane 3) or transfected with 3 × FLAG (lane 4). HepG2-hNTCP-C9-shPIN4-#1 cells were transfected with 3 × FLAG-Par14 WT (lane 5), 3 × FLAG-Par14-E46A/D74A (lane 6), 3 × FLAG-Par14-S19E (lane 7), 3 × FLAG-Par17 WT (lane 8), 3 × FLAG-Par17-E71A/D99A (lane 9), or 3 × FLAG-Par17-S44E (lane 10) **(D)**. **(E,F)** The HBc RP motif is critical for recruitment of HBc into cccDNA. HepG2-hNTCP-C9 (lane 1), HepG2-hNTCP-C9-shControl (lanes 2 and 3), and HepG2-hNTCP-C9-shPIN4-#1 (lanes 4 and 5) cells were infected with HBV WT (lanes 2 and 4) or HBV-HBc-AAP mutant (lanes 3 and 5) virions at 1.7×10^3 GEq per cell as detailed in the "Materials and Methods" section. (G) The HBc CTD is important for recruitment of HBc into cccDNA. HepG2-hNTCP-C9 (lane 1), HepG2-hNTCP-C9-shControl (lane 2), and HepG2-hNTCP-C9 *PIN4*-KD (lane 3) cells were used as controls. HepG2-hNTCP-C9 *PIN4*-KD cells were co-transfected with 3 × FLAG plus HBc WT (lane 4), the HBc CTD-deficient construct (lane 5), 3 × FLAG-Par14 WT plus HBc WT (lane 6) or the HBc CTD-deficient construct (lane 7), or 3 × FLAG-Par17 WT plus HBc WT (lane 8) or the HBc CTD-deficient construct (lane 9). HepG2-hNTCP-C9-shControl (lane 2) and HepG2-hNTCP-C9 *PIN4*-KD (lanes 3–9) cells were infected with HBV as described above. At 9 days p.i., chromatin solutions were prepared as described previously [35] and subjected to immunoprecipitation with an anti-PIN4, anti-FLAG, anti-HBc, anti-RNA polymerase II (Abcam #ab817), anti-acetyl H3 (Merck Millipore #06–599), or anti-H3 antibody (positive control) or normal rabbit polyclonal IgG (negative control). Immunoprecipitated chromatin was analyzed by semi-quantitative PCR **(A–E,G)** or quantitative real-time PCR **(F)**. Relative levels of HBc, RNA polymerase II, acetyl H3, and HBV RNA were measured using ImageJ 1.46r. Representative data from three independent experiments are shown. Statistical significance in E and F was evaluated using Student's *t*-test. $^*p < 0.05$ (E) and exact *p*-values **(F)** relative to the corresponding controls are shown.

H3 onto cccDNA (**Figure 9A**, third and fourth panels, lanes 2 vs. 3 and 4; Saeed et al., 2019). Furthermore, Par14/Par17 overexpression enhanced recruitment of HBc onto cccDNA (**Figure 9A**, top panel, lanes 2 vs. 3 and 4). *PIN4* KD reduced recruitment onto cccDNA (**Figure 9B**, top, third, and fourth panels, lanes 3 vs. 4 and 5).

To assess whether the substrate- and DNA-binding residues of Par14/Par17 (Saeed et al., 2019) are involved in recruitment of HBc onto cccDNA, ChIP was subjected (**Figure 9C**). Recruitment of HBc onto cccDNA was reduced by Par14-E46A/D74A, Par14-S19E, Par17-E71A/D99A, and Par17-S44E compared with Par14 WT and Par17 WT (**Figure 9C**, top panel, lanes 3 vs. 4 and 5; lanes 6 vs. 7 and 8), indicating that the substrate-binding E46/D74 of Par14 and E71/D99 of Par17 and the DNA-binding S19 of Par14 and S44 of Par17 are important for HBc recruitment onto cccDNA. The same result was obtained when a similar experiment was conducted with *PIN4*-KD HepG2-hNTCP-C9 cells (**Figure 9D**, top panel, lanes 5 vs. 6 and 7; lanes 8 vs. 9 and 10), further strengthening our conclusion.

Is the Par14/Par17-interacting ^{133}RP^{134} motif of HBc important for its recruitment onto cccDNA? We performed ChIP. shControl and *PIN4*-KD HepG2-hNTCP-C9 cells were infected with virions from HBV WT- or HBV-HBc-AAP-transfected HepG2 cells (**Figures 9E,F**). Recruitment of HBc-AAP onto cccDNA was lower than that of HBc WT in control cells (**Figure 9E**, top panel, lane 2 vs. 3). Likewise, recruitment of HBc-AAP onto cccDNA was lower than that of HBc WT in *PIN4*-KD cells (**Figure 9E**, top panel, lane 4 vs. 5), indicating that the ^{133}RP^{134} motif of HBc is important for interactions of HBc, Par14/Par17, and cccDNA. To quantitate recruitment of HBc WT and HBc-AAP onto cccDNA in the presence of absence of Par14/Par17, quantitative real-time PCR was performed (**Figure 9F**). As expected, recruitment of HBc-AAP was lower than that of HBc WT in shControl and *PIN4*-KD cells (**Figure 9F**, lane 2 vs. 3; lane 4 vs. 5). In the absence of Par14/Par17, the reduced recruitment of HBc-AAP relative to HBc WT was more evident, with ratios of 100:85 vs. 61:47 (100:67; **Figure 9F**, lane 2 vs. 3; lane 4 vs. 5).

The HBc CTD contains highly basic residues (arginine-rich, protamine-like) that resemble histone tails and are critical for non-specific nucleic acid binding (Nassal, 1990; Yu and Summers, 1991; Hatton et al., 1992; Köck et al., 2004; Jung et al., 2012, 2014; Diab et al., 2018). Therefore, the CTD of HBc may bind to cccDNA and the RP motif of HBc may interact with Par14/Par17. To explore this possibility, we used a HBc CTD-deficient construct (Jung et al., 2012). Co-transfected *PIN4*-KD HepG2-hNTCP-C9 cells were then infected with HBV WT, as described previously (Yang et al., 2019). Here, HBc proteins were provided by transfection and infection (**Figure 9G**). Therefore, in the case of CTD-deficient HBc transfection, both CTD-deficient HBc and HBc WT proteins were present (Yang et al., 2019). Transfection of CTD-deficient HBc reduced recruitment of HBc onto cccDNA in the presence or absence of Par14/Par17 WT (**Figure 9G**, top panel, lane 4 vs. 5; lane 6 vs. 7; lane 8 vs. 9). Since CTD-deficient HBc lacks NLS, it cannot localize in the nucleus. However, when both HBc WT and CTD-deficient HBc is present, HBc WT recruitment onto cccDNA is reduced, indicating that CTD-deficient HBc might interfere HBc WT to localize in the nucleus with unknown mechanism, resulting the reduced recruitment of HBc WT onto cccDNA. As expected, Par14/Par17 overexpression upregulated recruitment of HBc WT and CTD-deficient HBc onto cccDNA (**Figure 9G** top

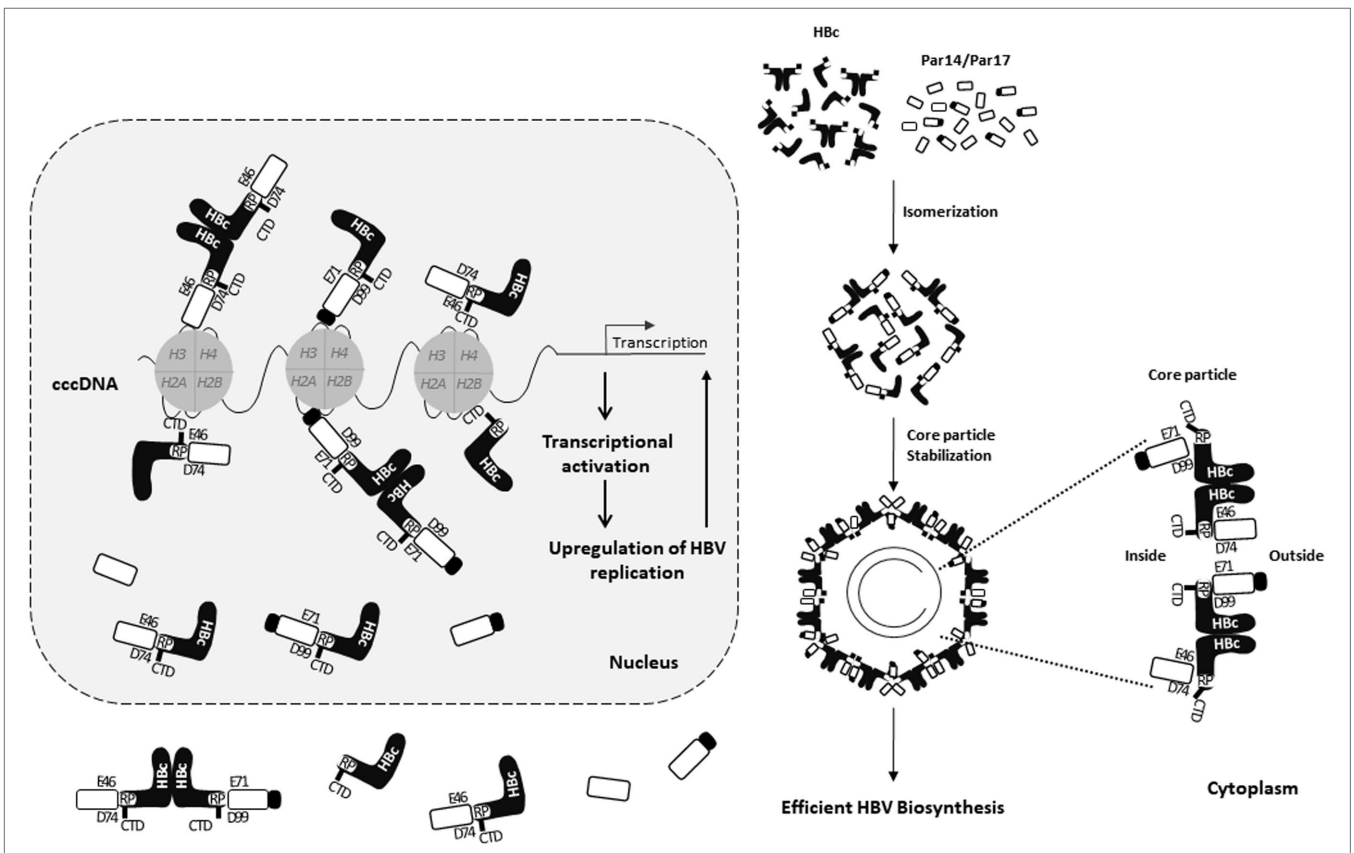

FIGURE 10 | Model of Par14/Par17–core particle interactions in the cytoplasm and interactions of Par14/Par17, HBc, and cccDNA in the nucleus. The HBV cccDNA minichromosome is associated with histone and non-histone cellular and viral proteins including HBc and HBx. In the nucleus, HBc binds to cccDNA and Par14/Par17 through its CTD and ^{133}RP^{134} motif, respectively. Par14 and Par17 in the nucleus also directly bind to cccDNA *via* S19 and S44, respectively, interact with HBc *via* the substrate-binding E46/D74 and E71/D99 residues, respectively, and promote recruitment of HBc into cccDNA. In the cytoplasm, Par14/Par17 bind to and stabilize HBc and enhance assembly and stability of the core particle by binding both outside and inside the core particle. Through these interactions in the nucleus and cytoplasm, HBV replication is upregulated.

panel, lane 4 vs. 6 and 8; lane 5 vs. 7 and 9), demonstrating that the CTD of HBc, in addition to its RP motif, is critical for recruitment of HBc onto cccDNA.

The E46/D74 and E71/D99 residues of Par14/Par17 bind to the ^{133}RP^{134} motif of HBc, the S19/44 residues of Par14/Par17 bind to cccDNA (Saeed et al., 2019), and the CTD of HBc binds to cccDNA (Chong et al., 2017). Therefore, HBc–Par14/Par17–cccDNA, HBc–cccDNA–Par14/Par17, or Par14/Par17–HBc–cccDNA interactions may occur in the nucleus (**Figure 10**).

Taken together, in addition to HBx–Par14/Par17–cccDNA interactions in the nucleus and HBx–Par14/Par17 interactions in the cytoplasm and mitochondria (Saeed et al., 2019), we demonstrate that interactions of HBc, Par14/Par17, and cccDNA in the nucleus and core particle–Par14/Par17 interactions in the cytoplasm can enhance HBV replication through increased transcriptional activity, increased core particle assembly and/or stability, and increased HBV DNA synthesis.

DISCUSSION

Host PPIase parvulins affect HBV. Specifically, Par14/Par17 interact with two RP motifs of HBx to enhance HBx stability and promote HBV replication (Saeed et al., 2019), Pin1 interacts with phosphorylated SP motifs of HBx to facilitate HBx transactivation and hepatocarcinogenesis progression (Pang et al., 2007), and Pin1 binds to HBc *via* specific phosphorylated Thr^{160}-Pro and Ser^{162}-Pro motifs and stabilizes HBc in a phosphorylation-dependent manner for efficient HBV propagation (Nishi et al., 2020). We demonstrate here that other parvulin proteins, Par14/Par17, physically interact with HBc protein, as shown using core particle assembly-defective HBc-Y132A (**Figure 1**) and stabilize HBc through its ^{133}RP^{134} motif (**Figure 6** and **Supplementary S7 Figure**). We further show that Par14/Par17 physically interact with the core particle (**Figure 1**) and enhance its stability through the HBc RP motif (**Figure 6**).

Several host factors reportedly bind to HBc and affect the stabilities of HBc and/or the core particle. Pin1 stabilizes HBc but it is unknown whether it affects core particle stability (Nishi et al., 2020). Heat shock protein 90 (hsp90) binds to the HBc-149 dimer and increases core particle stability (Shim et al., 2011). NIRF, an E3 ubiquitin ligase, and hsp40/DnaJ proteins bind to HBc and decrease its stability *via* unknown binding sites (Sohn et al., 2006; Qian et al., 2012).

Likewise, the HBc CTD phosphorylation status affects core particle stability (Selzer and Zlotnick, 2015). Although many HBc CTD-binding proteins have been identified (Diab et al., 2018; Yang, 2018), not many HBc NTD-binding proteins are known. Although hsp90 and NIRF are speculated to be HBc NTP-binding proteins, the exact HBc-binding sites have not been identified (Shim et al., 2011; Qian et al., 2012). We present Par14/Par17 as HBc NTD-binding proteins that enhance HBV replication and have multiple roles (**Figures 6–10**; Saeed et al., 2019).

Structural studies of HBc revealed that the RP motif is located in an irregular proline-rich loop 6 (^{128}TPPAY*RP*PN^{136}) followed by helix α5 (aa 112–127; Wynne et al., 1999). Loop 6 is highly conserved among 10 genotypes of human and mammalian hepadnaviruses (**Figures 3A,B**). In this loop, Y132 mediates the HBc dimer–dimer interaction to facilitate core particle assembly, meaning the Y132A mutant is core particle assembly-defective (Wynne et al., 1999; Bourne et al., 2009). Similarly, the HBc-R133D and -R133E mutants were core particle assembly-defective (**Figure 4**) and dimer-positive (**Figure 5C**), indicating that R133 is also involved in HBc dimer–dimer interactions to facilitate core particle formation. Of note, the Y132, R133, and P134 residues are completely conserved (**Figures 3A,B**).

The results of cryo-scanning electron microscopy indicated that the HBc CTD shuttles between the interior and exterior of the core particle (Yu et al., 2013), partly due to differences in its charge balance (Selzer et al., 2015). Unlike hsp90, which is incorporated into the core particle (Shim et al., 2011), the Nedd4 ubiquitin ligase and γ2-adaptin, a ubiquitin-interacting adaptor, may interact with the core particle partly through the surface-exposed, late domain-like ^{129}PPAY^{132} motif (Rost et al., 2006). Here, we show that some fractions of Par14/Par17 bind outside the core particle, while other fractions of Par14/Par17 are incorporated into the core particle (**Figure 2A**). Par14/Par17 bind to the HBc RP motif in the core particle (**Figures 4, 5A,B**) and the HBc PPAY motif is at the dimer–dimer interface (Wynne et al., 1999). Therefore, we propose that shuttling of the HBc CTD between the interior and exterior of the core particle (Wang et al., 2012; Yu et al., 2013) starts from loop 6, including the ^{129}PPAY^{132} and ^{133}RP^{134} motifs, to the structurally disordered HBc CTD.

A previous study demonstrated that core particles by the HBc-R133A mutant migrate rapidly by NAGE (Wu et al., 2018). We further showed that core particles by the HBc-R133L, -R133H, -AAP, and AAA mutants also migrate rapidly (**Figures 4B,C**, second and third panels, lanes 2 vs. 4, 8, 9, 11, and 13) and fail to interact with Par14/Par17 (**Figures 4B,C**, top panel, lanes 2 vs. 4, 8, 9, 11, and 13). Interestingly, when R133 is changed to negatively charged D or E, core particle assembly is defective, as observed with the HBc-Y132A mutant (**Figures 4B,C**, top panel, lanes 2 vs. 4, 8, 9, 11, and 13). The E46/71 and D74/99 residues of Par14/Par17 are important for interactions with HBc and the core particle (**Figures 2B–D**); therefore, the R133D or R133E HBc mutant may repel Par14/Par17, rendering core particle assembly-defective. Taken together, we suggest that a positively charged residue at position 133 of HBc at the surface of the core particle changes the mobility of the core particle and ensures it is neither too stable nor unstable for replication (Jung et al., 2012; Wu et al., 2018) and that this is assisted through interactions with Par14/Par17.

Nuclear HBc plays prominent roles in modulating viral and host gene expression, splicing and nuclear export of viral transcripts, and cccDNA function.[7] HBc is a main component of HBV cccDNA (Bock et al., 2001; Guo et al., 2011; Lucifora and Protzer, 2016; Diab et al., 2018). HBc induces nucleosomal organization to positively regulate HBV transcription (Bock et al., 2001; Guo et al., 2011). However, HBc may not be absolutely required for cccDNA transcription (Zhang et al., 2014). Furthermore, repressive symmetric dimethylation of R3 of H4 (H4R3me2s) on cccDNA by PRMT5 occurs through its interaction with HBc (Zhang et al., 2017). Conversely, HBc positively regulates

HBV transcription through the interaction of its RP motif with Par14/Par17 (**Figures 8, 9** and **Supplementary Figures S12–S15**). Taken together, we postulate that HBc can function as both a negative and positive regulator of HBV transcription through its interactions with repressive modifiers, such as PRMT5, and activating modifiers, such as CREB-binding protein (Guo et al., 2011) and Par14/Par17 (**Figures 8–10**).

Consistent with the structural and regulatory roles of HBc in HBV replication (Zlotnick et al., 2015; Diab et al., 2018), our study further demonstrated that Par14/Par17 strengthen the structural roles of HBc and the core particle by enhancing their stabilities (**Figure 6**). The cccDNA–Par14/17–HBx complex promotes transcriptional activation (Saeed et al., 2019), and Par14/Par17 enhance recruitment of HBc into cccDNA and HBV transcription (**Figure 9** and **Supplementary Figures S12–S15**), strengthening the regulatory role of HBc. Taken together, we hypothesize that the chromatin remodelers Par14/Par17 induce unwinding of cccDNA *via* HBc and HBx proteins to activate transcription and ultimately augment HBV replication. This hypothesis should be investigated in the future. If this proves to be the case, targeting HBc, HBx, or Par14/Par17 might cure HBV infection by silencing cccDNA transcription.

Additionally, Iwamoto et al. (2017) demonstrated that microtubules are important for efficient HBV core particle formation and replication. Since Par14/Par17 can interact with tubulin and promote its polymerization (Thiele et al., 2011), whether Par14/Par17 facilitate HBV replication through an enhanced tubulin polymerization can be investigated in the future. Also, it should be investigated whether other HBV proteins, such as HBs or polymerase, might also interact with Par14/Par17 and affect HBV replication through their interaction.

Statistical Analysis

Data are expressed as mean values ± standard deviations. Mean values were compared using Student's *t*-test. Values of $p < 0.05$ were considered statistically significant.

DATA AVAILABILITY STATEMENT

The original contributions presented in the study are included in the article/**Supplementary Material**, further inquiries can be directed to the corresponding author.

AUTHOR CONTRIBUTIONS

KK: study concept and design, study supervision, analysis and interpretation of data, obtained funding, drafting of the manuscript, and critical revision of the manuscript. US: acquisition of data, analysis and interpretation of data, and drafting of the manuscript. ZP: analysis and interpretation of data and statistical analysis. HK, JK, and FK: administrative, technical, or material support. Y-JC, SP, H-JS, HL, and JL: critical revision of the manuscript. All authors contributed to the article and approved the submitted version.

FUNDING

This work was supported by the National Research Foundation Grants funded by the Korean Government (NRF-2019-R1A2C2005749).

AUTHOR SUMMARY

The essential HBc protein plays structural and regulatory roles for HBV replication. We demonstrated that parvulin Par14/Par17 proteins can bind to both HBc and core particle, through a conserved RP motif on HBc. Through HBc– and/or core particle–Par14/Par17 interactions, HBc and core particle can be stabilized, and HBV replication can be upregulated. Also, Par14/Par17 were shown to promote HBc recruitment into cccDNA, like HBx. Our results indicate that in addition to the HBx–Par14/Par17–cccDNA interaction in the nucleus, the triple HBc, Par14/Par17, and cccDNA interaction in the nucleus, and the core particle–Par14/Par17 interaction in the cytoplasm are also important for HBV replication. These results suggest that inhibition or knockdown of Par14/Par17 may control HBV infection.

SUPPLEMENTARY MATERIAL

The Supplementary Material for this article can be found online at: https://www.frontiersin.org/articless/10.3389/fmicb.2021.795047/full#supplementary-material

REFERENCES

Belloni, L., Pollicino, T., de Nicola, F., Guerrieri, F., Raffa, G., and Fanciulli, M., et al. (2009). Nuclear HBx binds the HBV minichromosome and modifies the epigenetic regulation of cccDNA function. Available at: www.pnas.org/cgi/content/full/ (Accessed November 26, 2021).

Birnbaum, F., and Nassal, M. (1990). Hepatitis B virus nucleocapsid assembly: primary structure requirements in the core protein. *J. Virol.* 64, 3319–3330. doi: 10.1128/JVI.64.7.3319-3330.1990

Bock, C. T., Schwinn, S., Locarnini, S., Fyfe, J., Manns, M. P., and Trautwein, C. (2001). Structural organization of the hepatitis B virus minichromosome. *J. Mol. Biol.* 307, 183–196. doi: 10.1006/jmbi.2001.4481

Bourne, C. R., Katen, S. P., Fulz, M. R., Packianathan, C., and Zlotnick, A. (2009). A mutant hepatitis B virus core protein mimics inhibitors of icosahedral capsid self-assembly. *Biochemistry* 48, 1736–1742. doi: 10.1021/bi801814y

Cai, D., Nie, H., Yan, R., Guo, J.-T., Block, T. M., and Guo, H. (2013). A southern blot assay for detection of hepatitis B virus covalently closed circular DNA from cell cultures. *Methods Mol Biol.* 1030, 151–161. doi: 10.1007/978-1-62703-484-5_13

Chao, S.-H., Greenleaf, A. L., and Price, D. H. (2001). Juglone, an inhibitor of the peptidyl-prolyl isomerase pin1, also directly blocks transcription. *Nucleic Acids Res.* 29, 767–773. doi: 10.1093/nar/29.3.767

Chong, C. K., Cheng, C. Y. S., Tsoi, S. Y. J., Huang, F. Y., Liu, F., Seto, W. K., et al. (2017). Role of hepatitis B core protein in HBV transcription and recruitment of histone acetyltransferases to cccDNA minichromosome. *Antivir. Res.* 144, 1–7. doi: 10.1016/j.antiviral.2017.05.003

CLC Main workbench 21.0 software (2021). CLC Main workbench 8 software. Available at: https://www.qiagenbioinformatics.com/products/clc-main-workbench/ (Accessed October 1, 2021).

Cold Spring Harbor Laboratory (2015a). SDS–PAGE Sample Buffer (Nonreducing), Cold Spring Harb Protocol. Available at: http://cshprotocols.cshlp.org/content/2015/5/pdb.rec086991.full?rss=1 (Accessed October 1, 2021).

Cold Spring Harbor Laboratory (2015b). SDS–PAGE Sample Buffer (Reducing), Cold Spring Harb Protocol. Available at: http://cshprotocols.cshlp.org/content/2015/5/pdb.rec086942.full?text_only=true (Accessed October 1, 2021).

Cornberg, M., and Manns, M. P. (2018). Hepatitis: No cure for hepatitis B and D without targeting integrated viral DNA? *Nat. Rev. Gastroenterol. Hepatol.* 15, 195–196. doi: 10.1038/nrgastro.2017.185

Diab, A., Foca, A., Zoulim, F., Durantel, D., and Andrisani, O. (2018). The diverse functions of the hepatitis B core/capsid protein (HBc) in the viral life cycle: implications for the development of HBc-targeting antivirals. *Antivir. Res.* 149, 211–220. doi: 10.1016/j.antiviral.2017.11.015

Gallina, A., Bonelli, F., Zentilin, L., Rindi, G., Muttini, M., and Milanesi, G. (1989). A recombinant hepatitis B core antigen polypeptide with the protamine-like domain deleted self-assembles into capsid particles but fails to bind nucleic acids. *J. Virol.* 63, 4645–4652. doi: 10.1128/JVI.63.11.4645-4652.1989

Ganem, D. S. R. J. (2001). "The molecular biology of the hepatitis B viruses," in *Fields Virology. 4th Edn*. ed. Knipe (Philadelphia: Lippincott Williams & Wilkins).

Göthel, S. F., and Marahiel, M. A. (1999). Review peptidyl-prolyl cis-trans isomerases, a superfamily of Ubiquitous folding catalysts. *Cell Mol. Life Sci.* 55, 423–436. doi: 10.1007/s000180050299

Guo, Y. H., Li, Y. N., Zhao, J. R., Zhang, J., and Yan, Z. (2011). HBc binds to the CpG islands of HBV cccDNA and promotes an epigenetic permissive state. *Epigenetics* 6, 720–726. doi: 10.4161/epi.6.6.15815

Hatton, T., Zhou, S., and Standringl, D. N. (1992). RNA-and DNA-binding activities in hepatitis B virus capsid protein: a model for their roles in viral replication. *J. Virol.* 66, 5232–5241. doi: 10.1128/JVI.66.9.5232-5241.1992

Hennig, L., Christner, C., Kipping, M., Schelbert, B., Rücknagel, K. P., Grabley, S., et al. (1998). Selective inactivation of parvulin-like peptidyl-prolyl cis/trans isomerases by juglone. *Biochemistry* 37, 5953–5960. doi: 10.1021/bi973162p

Hu, J., and Seeger, C. (2015). Hepadnavirus genome replication and persistence. *Cold Spring Harb. Perspect. Med.* 5:a021386. doi: 10.1101/cshperspect.a021386

Iwamoto, M., Cai, D., Sugiyama, M., Suzuki, R., Aizaki, H., Ryo, A., et al. (2017). Functional association of cellular microtubules with viral capsid assembly supports efficient hepatitis B virus replication. *Sci. Rep.* 7:10620. doi: 10.1038/s41598-017-11015-4

Jung, J., Hwang, S. G., Chwae, Y.-J., Park, S., Shin, H.-J., and Kim, K. (2014). Phosphoacceptors threonine 162 and serines 170 and 178 within the carboxyl-terminal RRRS/T motif of the hepatitis B virus core protein make multiple contributions to hepatitis B virus replication. *J. Virol.* 88, 8754–8767. doi: 10.1128/jvi.01343-14

Jung, J., Kim, H.-Y., Kim, T., Shin, B.-H., Park, G.-S., Park, S., et al. (2012). C-terminal substitution of HBV core proteins with those from DHBV reveals that arginine-rich 167RRRSQSPRR175 domain is critical for HBV replication. *PLoS One* 7:e41087. doi: 10.1371/journal.pone.0041087

Kim, H. Y., Kim, H. Y., Jung, J., Park, S., Shin, H. J., and Kim, K. (2008). Incorporation of deoxyribonucleotides and ribonucleotides by a dNTP-binding cleft mutated reverse transcriptase in hepatitis B virus core particles. *Virology* 370, 205–212. doi: 10.1016/j.virol.2007.08.018

Kim, H. Y., Park, G. S., Kim, E. G., Kang, S. H., Shin, H. J., Park, S., et al. (2004). Oligomer synthesis by priming deficient polymerase in hepatitis B virus core particle. *Virology* 322, 22–30. doi: 10.1016/j.virol.2004.01.009

Ko, C., Chakraborty, A., Chou, W. M., Hasreiter, J., Wettengel, J. M., Stadler, D., et al. (2018). Hepatitis B virus genome recycling and de novo secondary infection events maintain stable cccDNA levels. *J. Hepatol.* 69, 1231–1241. doi: 10.1016/j.jhep.2018.08.012

Köck, J., Nassal, M., Deres, K., Blum, H. E., and von Weizsäcker, F. (2004). Hepatitis B virus nucleocapsids formed by carboxy-terminally mutated core proteins contain spliced viral genomes but lack full-size DNA. *J. Virol.* 78, 13812–13818. doi: 10.1128/jvi.78.24.13812-13818.2004

Liu, K., Luckenbaugh, L., Ning, X., Xi, J., and Hu, J. (2018). Multiple roles of core protein linker in hepatitis B virus replication. *PLoS Pathog.* 14:e1007085, 29782550. doi: 10.1371/journal.ppat.1007085

Lu, K. P., Finn, G., Lee, T. H., and Nicholson, L. K. (2007). Prolyl cis-trans isomerization as a molecular timer. *Nat. Chem. Biol.* 3, 619–629. doi: 10.1038/nchembio.2007.35

Lu, K. P., Hanes, S. D., and Hunter, T. (1996). A human peptidyl–prolyl isomerase essential for regulation of mitosis. *Nature* 380, 544–547. doi: 10.1038/380544a0

Lucifora, J., and Protzer, U. (2016). Attacking hepatitis B virus cccDNA-The holy grail to hepatitis B cure. *J. Hepatol.* 64, S41–S48. doi: 10.1016/j.jhep.2016.02.009

Matena, A., Rehic, E., Hönig, D., Kamba, B., and Bayer, P. (2018). Structure and function of the human parvulins Pin1 and Par14/17. *Biol. Chem.* 399, 101–125. doi: 10.1515/hsz-2017-0137

Mohd-Ismail, N. K., Lim, Z., Gunaratne, J., and Tan, Y. J. (2019). Mapping the interactions of HBV cccDNA with host factors. *Int. J. Mol. Sci.* 20:4276. doi: 10.3390/ijms20174276

Mueller, J. W., Kessler, D., Neumann, D., Stratmann, T., Papatheodorou, P., Hartmann-Fatu, C., et al. (2006). Characterization of novel elongated Parvulin isoforms that are ubiquitously expressed in human tissues and originate from alternative transcription initiation. *BMC Mol. Biol.* 7:9. doi: 10.1186/1471-2199-7-9

Nassal, M. (1990). Hepatitis B Virus nucleocapsid assembly: primary structure requirements in the core protein. *J. Virol.* 64, 3319–3330. doi: 10.1006/jmbi.2000.4481

Nassal, M. (1992). The arginine-rich domain of the hepatitis B virus core protein is required for pregenome encapsidation and productive viral positive-strand DNA synthesis but not for virus assembly. *J. Virol.* 66, 4107–4116. doi: 10.1128/JVI.66.7.4107-4116.1992

Ni, Y., Lempp, F. A., Mehrle, S., Nkongolo, S., Kaufman, C., Fälth, M., et al. (2014). Hepatitis B and D viruses exploit sodium taurocholate co-transporting polypeptide for species-specific entry into hepatocytes. *Gastroenterology* 146, 1070–1083. doi: 10.1053/j.gastro.2013.12.024

Nishi, M., Miyakawa, K., Matsunaga, S., Khatun, H., Yamaoka, Y., Watashi, K., et al. (2020). Prolyl isomerase Pin1 regulates the stability of hepatitis B virus core protein. *Front. Cell Dev. Biol.* 8:26. doi: 10.3389/fcell.2020.00026

Nkongolo, S., Ni, Y., Lempp, F. A., Kaufman, C., Lindner, T., Esser-Nobis, K., et al. (2014). Cyclosporin A inhibits hepatitis B and hepatitis D virus entry by cyclophilin-independent interference with the NTCP receptor. *J. Hepatol.* 60, 723–731. doi: 10.1016/j.jhep.2013.11.022

Pang, R., Lee, T. K. W., Poon, R. T. P., Fan, S. T., Wong, K. B., Kwong, Y. L., et al. (2007). Pin1 interacts with a specific serine-proline motif of hepatitis B virus X-protein to enhance hepatocarcinogenesis. *Gastroenterology* 132, 1088–1103. doi: 10.1053/j.gastro.2006.12.030

Piracha, Z. Z., Kwon, H., Saeed, U., Kim, J., Jung, J., Chwae, Y.-J., et al. (2018). Sirtuin 2 isoform 1 enhances hepatitis B virus RNA transcription and DNA synthesis through the AKT/GSK-3β/β-catenin signaling pathway. *J. Virol.* 92:e00955-18. doi: 10.1128/jvi.00955-18

Piracha, Z. Z., Saeed, U., Kim, J., Kwon, H., Chwae, Y.-J., Lee, H. W., et al. (2020). An alternatively spliced sirtuin 2 isoform 5 inhibits hepatitis B virus replication from cccDNA by repressing epigenetic modifications made by histone lysine methyltransferases. *J. Virol.* 94:e00926-20. doi: 10.1128/jvi.00926-20

Qian, G., Jin, F., Chang, L., Yang, Y., Peng, H., and Duan, C. (2012). NIRF, a novel ubiquitin ligase, interacts with hepatitis B virus core protein and promotes its degradation. *Biotechnol. Lett.* 34, 29–36. doi: 10.1007/s10529-011-0751-0

Revill, P. A., Chisari, F. V., Block, J. M., Dandri, M., Gehring, A. J., Guo, H., et al. (2019). A global scientific strategy to cure hepatitis B. *Lancet Gastroenterol. Hepatol.* 4, 545–558. doi: 10.1016/S2468-1253(19)30119-0

Rost, M., Mann, S., Lambert, C., Döring, T., Thomé, N., and Prange, R. (2006). γ2-adaptin, a novel ubiquitin-interacting adaptor, and Nedd4 ubiquitin ligase control hepatitis B virus maturation. *J. Biol. Chem.* 281, 29297–29308. doi: 10.1074/jbc.M603517200

Rulten, S., Thorpe, J., and Kay, J. (1999). Identification of eukaryotic Parvulin homologues: A new subfamily of Peptidylprolyl cis-trans Isomerases 1. Available at: http://www.idealibrary.com (Accessed November 26, 2021).

Saeed, U., Kim, J., Piracha, Z. Z., Kwon, H., Jung, J., Chwae, Y.-J., et al. (2019). Parvulin 14 and parvulin 17 bind to HBx and cccDNA and upregulate hepatitis B virus replication from cccDNA to virion in an HBx-dependent manner. *J. Virol.* 93:e01840-18. doi: 10.1128/jvi.01840-18

Saningong, A. D., and Bayer, P. (2015). Human DNA-binding peptidyl-prolyl cis/trans isomerase Par14 is cell cycle dependently expressed and associates with chromatin in vivo. *BMC Biochem.* 16:4. doi: 10.1186/s12858-015-0033-x

Seeger, C., and Mason, W. S. (2015). Molecular biology of hepatitis B virus infection. *Virology* 479–480, 672–686. doi: 10.1016/j.virol.2015.02.031

Selzer, L., Kant, R., Wang, J. C. Y., Bothner, B., and Zlotnick, A. (2015). Hepatitis B virus core protein phosphorylation sites affect capsid stability and transient exposure of the C-terminal domain. *J. Biol. Chem.* 290, 28584–28593. doi: 10.1074/jbc.M115.678441

Selzer, L., and Zlotnick, A. (2015). Assembly and release of hepatitis B virus. *Cold Spring Harb. Perspect. Med.* 5:a021394. doi: 10.1101/cshperspect.a021394

Shim, H. Y., Quan, X., Yi, Y. S., and Jung, G. (2011). Heat shock protein 90 facilitates formation of the HBV capsid via interacting with the HBV core protein dimers. *Virology* 410, 161–169. doi: 10.1016/j.virol.2010.11.005

Sohn, S. Y., Kim, S. B., Kim, J., and Ahn, B. Y. (2006). Negative regulation of hepatitis B virus replication by cellular Hsp40/DnaJ proteins through destabilization of viral core and X proteins. *J. Gen. Virol.* 87, 1883–1891. doi: 10.1099/vir.0.81684-0

Thiele, A., Krentzlin, K., Erdmann, F., Rauh, D., Hause, G., Zerweck, J., et al. (2011). Parvulin 17 promotes microtubule assembly by its peptidyl-prolyl cis/trans isomerase activity. *J. Mol. Biol.* 411, 896–909. doi: 10.1016/j.jmb.2011.06.040

Uchida, T., Takamiya, M., Takahashi, M., Miyashita, H., Ikeda, H., Terada, T., et al. (2003). Pin1 and Par14 peptidyl prolyl isomerase inhibitors block cell proliferation. *Chem. Biol.* 10, 15–24. doi: 10.1016/S

Venkatakrishnan, B., and Zlotnick, A. (2016). The structural biology of hepatitis B virus: form and function. *Annu. Rev. Virol.* 3, 429–451. doi: 10.1146/annurev-virology-110615-042238

Wang, J. C. Y., Dhason, M. S., and Zlotnick, A. (2012). Structural organization of pregenomic RNA and the carboxy-terminal domain of the capsid protein of hepatitis B virus. *PLoS Pathog.* 8:e1002919. doi: 10.1371/journal.ppat.1002919

Watashi, K., Liang, G., Iwamoto, M., Marusawa, H., Uchida, N., Daito, T., et al. (2013). Interleukin-1 and tumor necrosis factor-α trigger restriction of hepatitis B virus infection via a cytidine deaminase activation-induced cytidine deaminase (AID). *J. Biol. Chem.* 288, 31715–31727. doi: 10.1074/jbc.M113.501122

Watts, N. R., Conway, J. F., Cheng, N., Stahl, S. J., Belnap, D. M., Steven, A. C., et al. (2002). The morphogenic linker peptide of HBV capsid protein forms a mobile array on the interior surface. *EMBO J.* 21, 876–884. doi: 10.1093/emboj/21.5.876

World Health Organization Gobal Heptatitis report (2017). Global hepatitis report, 2017. Available at: http://www.who.int/hepatitis/publications/global-hepatitis-report2017/en/ (Accessed November 26, 2021).

Wu, S., Luo, Y., Viswanathan, U., Kulp, J., Cheng, J., Hu, Z., et al. (2018). CpAMs induce assembly of HBV capsids with altered electrophoresis mobility: implications for mechanism of inhibiting pgRNA packaging. *Antivir. Res.* 159, 1–12. doi: 10.1016/j.antiviral.2018.09.001

Wynne, S. A., Crowther, R. A., and Leslie, A. G. W. (1999). The crystal structure of the human hepatitis B virus capsid. *Mol. Cell.* 3, 771–780. doi: 10.1016/s1097-2765(01)80009-5

Xie, Q., Fan, F., Wei, W., Liu, Y., Xu, Z., Zhai, L., et al. (2017). Multi-omics analyses reveal metabolic alterations regulated by hepatitis B virus core protein in hepatocellular carcinoma cells. *Sci. Rep.* 7:41089. doi: 10.1038/srep41089

Yan, H., Zhong, G., Xu, G., He, W., Jing, Z., Gao, Z., et al. (2012). Sodium taurocholate cotransporting polypeptide is a functional receptor for human hepatitis B and D virus. *Elife* 1:e00049. doi: 10.7554/eLife.00049

Yang, F. (2018). Post-translational modification control of HBV biological processes. *Front. Microbiol.* 9:2661. doi: 10.3389/fmicb.2018.02661

Yang, G., Feng, J., Liu, Y., Zhao, M., Yuan, Y., Yuan, H., et al. (2019). HAT1 signaling confers to assembly and epigenetic regulation of HBV cccDNA minichromosome. *Theranostics* 9, 7345–7358. doi: 10.7150/thno.37173

Yoon, S., Jung, J., Kim, T., Park, S., Chwae, Y. J., Shin, H. J., et al. (2011). Adiponectin, a downstream target gene of peroxisome proliferator-activated receptor γ, controls hepatitis B virus replication. *Virology* 409, 290–298. doi: 10.1016/j.virol.2010.10.024

Yu, X., Jin, L., Jih, J., Shih, C., and Hong Zhou, Z. (2013). 3.5Å cryoEM structure of hepatitis B virus core assembled from full-length core protein. *PLoS One*:e69729, 8. doi: 10.1371/journal.pone.0069729

Yu, M., and Summers, J. (1991). A domain of the hepadnavirus capsid protein is specifically required for DNA maturation and virus assembly. *J. Virol.* 65, 2511–2517. doi: 10.1128/JVI.65.5.2511-2517.199

Zhang, W., Chen, J., Wu, M., Zhang, X., Zhang, M., Yue, L., et al. (2017). PRMT5 restricts hepatitis B virus replication through epigenetic repression of covalently closed circular DNA transcription and interference with pregenomic RNA encapsidation. *Hepatology* 66, 398–415. doi: 10.1002/hep.29133/suppinfo

Zhang, Y., Mao, R., Yan, R., Cai, D., Zhang, Y., Zhu, H., et al. (2014). Transcription of hepatitis B virus covalently closed circular DNA is regulated by CpG methylation during chronic infection. *PLoS One* 9:e110442. doi: 10.1371/journal.pone.0110442

Zlotnick, A., Cheng, N., Conway, J. F., Booy, F. P., Steven, A. C., and Stahl, S. J. (1996). et al, Dimorphism of hepatitis B virus capsids is strongly influenced by the c-terminus of the capsid protein. *Biochemistry* 35, 7412–7421. doi: 10.1021/bi9604800

Zlotnick, A., Venkatakrishnan, B., Tan, Z., Lewellyn, E., Turner, W., and Francis, S. (2015). Core protein: A pleiotropic keystone in the HBV lifecycle. *Antivir. Res.* 121, 82–93. doi: 10.1016/j.antiviral.2015.06.020

Conflict of Interest: The authors declare that the research was conducted in the absence of any commercial or financial relationships that could be construed as a potential conflict of interest.

Publisher's Note: All claims expressed in this article are solely those of the authors and do not necessarily represent those of their affiliated organizations, or those of the publisher, the editors and the reviewers. Any product that may be evaluated in this article, or claim that may be made by its manufacturer, is not guaranteed or endorsed by the publisher.